Title

Flux-driven algebraic damping of m=1 diocotron mode

Journal

Physics of Plasmas, 23(7)

ISSN

1070-664X 1089-7674

Authors

Chim, Chi Yung

O'Neil, Thomas M

Publication Date

2016-07-01

DOI

10.1063/1.4958317

Data Availability

The data associated with this publication are available upon request.

Peer reviewed

Flux-driven algebraic damping of $m = 1$ diocotron mode

Chi Yung Chim and Thomas M. O'Neil[1]

University of California at San Diego, La Jolla, California 92093

(Dated: 24 May 2016)

Recent experiments with pure electron plasmas in a Malmberg-Penning trap have observed the algebraic damping of $m = 1$ diocotron modes. Transport due to small field asymmetries produces a low density halo of electrons moving radially outward from the plasma core, and the mode damping begins when the halo reaches the resonant radius $r = R_w$ at the wall of the trap. The damping rate is proportional to the flux of halo particles through the resonant layer. The damping is related to, but distinct from spatial Landau damping, in which a linear wave-particle resonance produces exponential damping. This paper explains with analytic theory the new algebraic damping due to particle transport by both mobility and diffusion. As electrons are swept around the "cat's eye" orbits of the resonant wave-particle interaction, they form a dipole ($m = 1$) density distribution. From this distribution, the electric field component perpendicular to the core displacement produces $\mathbf{E} \times \mathbf{B}$-drift of the core back to the axis, that is, damps the $m = 1$ mode. The parallel component produces drift in the azimuthal direction, that is, causes a shift in the mode frequency.

This manuscript was accepted by Phys. Plasmas. Click here to see the version of record.

I. INTRODUCTION

Diocotron modes are dominant features in the low frequency dynamics of nonneutral plasmas confined in Malmberg-Penning traps[1–4]. In an ideal limit, these modes involve only cross magnetic field $\mathbf{E} \times \mathbf{B}$ drift motion and are described by the drift-Poisson equations[1]. These equations are isomorphic to Euler's equations for the ideal (i.e., incompressible and inviscid) flow of a neutral fluid, and the diocotron modes are analogues of a Kelvin modes on a fluid vortex[5].

There has been much previous work on diocotron mode instabilities[2,6–8] and on diocotron mode damping[5,9–12]. This paper focus on damping.

Previously identified damping mechanisms include a spatial version of the Landau resonance[5,9], the rotational pumping of bulk viscosity[10,11], axial velocity dissipation on a separatrix for plasma columns with trapped and passing particles[13], and a strong damping mechanism when the radial magnetron field from end cylinders dominates over the radial space charge field[12]. The Landau mechanism fits into the ideal 2D $\mathbf{E} \times \mathbf{B}$ drift framework, but others, such as rotational pumping, involve physics beyond the ideal model.

This paper discusses a damping mechanism that is a close cousin of Landau damping, so we begin with a review of the spatial Landau resonance.

The nonneutral plasma column is immersed in a uniform axial magnetic field $B\hat{z}$, has a radial space charge electric field $E(r)\hat{r}$, and consequently undergoes an azimuthal $\mathbf{E} \times \mathbf{B}$ drift rotation. Here, (r, θ, z) is a cylindrical coordinate system with the z-axis coincident with the axis of the trap. We consider the plasma column to be a pure electron plasma in this paper.

A diocotron mode of azimuthal mode number m can experience a resonant interaction with the rotating plasma flow at a critical plasma radius $R_{\rm res}(m)$, where $\omega_m = m\omega_E[R_{\rm res}(m)]$. Here, m is the azimuthal mode number, ω_m is the mode frequency, and $\omega_E(r) = -cE(r)/Br$ is the local rotation frequency of the plasma.

Linear mode theory[5,9] predicts that this spatial Landau resonance produces exponential mode damping when the slope of the radial density distribution is negative at the critical radius, and this damping has been observed experimentally for low order azimuthal modes with $m > 1$[9].

The $m = 1$ mode is special in that the resonant radius is at the wall where typically there

ing no particles. It was long thought that an $m = 1$ mode would not experience damping due to a Landau resonance[5].

However, recent experiments[14] have observed a novel algebraic damping of the $m = 1$ mode, which we believe is a close cousin of Landau damping. In these experiments, transport produces a low density halo of particles that gradually extends out from the plasma core until it reaches the wall. The algebraic damping begins when the halo reaches the resonant region (the wall for $m = 1$), and the damping rate is proportional to the flux of particles through the resonance.

The theoretical picture that we envision for this flux driven algebraic damping is similar to, but distinct from, spatial Landau damping. In both cases, the damping results from an interaction of the mode field with resonant particles, but the particulars of the interactions are very different in the two cases. In spatial Landau damping, the resonant particles are present before the mode is excited, and the damping results from a mode-driven rearrangement of particles near the resonant radius. The analysis is linear and leads to exponential damping.

In contrast, for the new flux-driven algebraic damping, there are no particles initially at the resonant radius. The transport gradually brings particles to the resonant radius, and the mode field then sweeps the particles around the nonlinear cat's eye orbits to a scrape-off layer, causing the damping.

As will be discussed later, the scrape-off layer is a thin region adjacent to the wall where guiding center drift theory breaks down and particles (electrons) are rapidly absorbed by the wall. The scrape-off layer is at least as thick as a cyclotron radius. We will assume that the thickness of the layer is much smaller than the mode amplitude.

While the new theory can be described within a 2D flow framework, the transport and the truncation of particle orbits by the wall are non-ideal elements beyond the $\mathbf{E} \times \mathbf{B}$ drift description.

The paper that reported the experimental results on the new damping also included a short theoretical explanation[14,15]. To help understand this theory consider Fig. 1, which shows the cross section of an electron plasma column that has been displaced off the trap axis through the excitation of an $m = 1$ diocotron mode. The displacement is of magnitude D and direction $\bar{\theta} = 0$. The gray lines are equipotential contours as seen in the mode frame. In this frame the $\mathbf{E} \times \mathbf{B}$ drift flow is along the equipotential contours. The orange shaded

region represents the relatively high density plasma core. In this region, the mode potential can be described by linear theory, and the equipotential curves are simply displaced circles. The resonant region is near the wall, and there nonlinear effects distort the circles. Near the left side of the figure are the "cat's eye" orbits, which describe the motion of particles that are trapped in the wave trough. In order to make the "cat's eye" orbits easier to see in Fig. 1, the ratio of the displacement to the wall radius (i.e. D/R_w) was taken to be the largest of experiment values at 0.1.

In addition to the $\mathbf{E}\times\mathbf{B}$ drift flow, there is a slow transport flow. The transport produces a low density halo that gradually extends out from the plasma core. A given particle slowly spirals out, moving successively from one contour to another of larger radius.

The green dot-dashed equipotential contours in Fig. 1 is the critical contour that just misses the blue dashed scrape-off layer at $\bar{\theta} = 0$. When transport moves an electron through this critical contour, the electron hits the scrape-off layer and is absorbed by the wall before returning to $\bar{\theta} = 0$. The red solid curve in Fig. 1 shows the trajectory of such an electron.

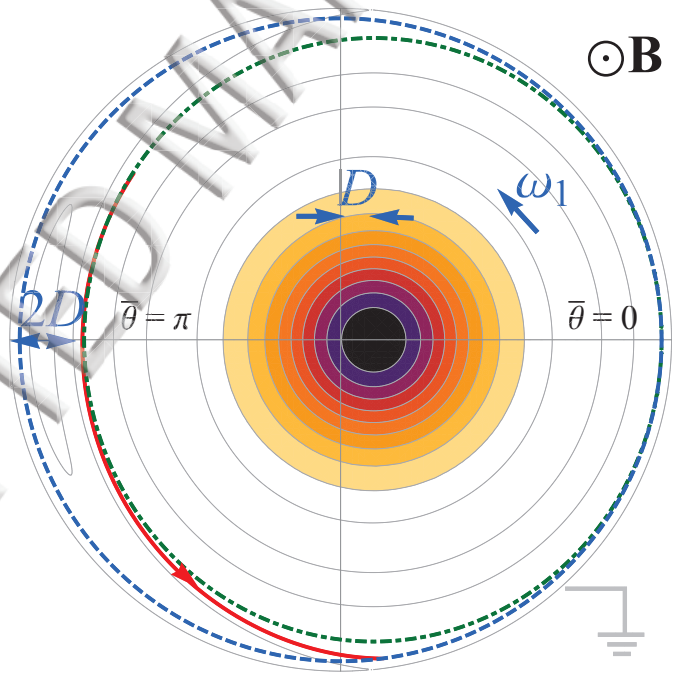

FIG. 1. Cross section of the electron plasma column in a $m = 1$ mode. The orange shaded region is the plasma core. The gray lines are equipotential contours in the mode frame. The blue dashed curve is the scrape-off layer. The green dot-dashed curve is the critical contour. The red solid curve is a particle trajectory.

The previous theory focuses on the transfer of canonical angular momenta from the plasma core to such electrons. In the guiding center drift approximation, the canonical angular momentum for an electron in the uniform magnetic field of the trap is simply $P_\theta = eBr^2/2c$, where the radial position r is measured from the center of the trap, B is the magnetic field strength and $e = -|e|$ is the electron charge[16,17]. When an $m = 1$ diocotron mode is excited, the plasma core is displaced off the trap axis by a small amount D, and the core canonical angular momentum per unit length is changed by $N(eB/2c)D^2$, where N is the number of core particles per unit length[9]. This change in angular momentum is called the canonical angular momentum of the mode.

When an individual electron $\mathbf{E} \times \mathbf{B}$ drifts in a nearly circular orbit around the displaced center of the plasma core, the radius of the electron measured from the center of the trap oscillates by order $\Delta r \sim D\cos[\bar{\theta}(t)]$. Thus, the electron continually trades angular momentum back and forth with the core, or equivalently with mode. However, the orbit for an electron that crosses the critical contour is truncated by the wall, so there is a net change in angular momentum. Since the thickness of the "cat's eye" orbit is of order D, the net change in angular momentum is of order $\Delta P_\theta \sim (eB/2c)[R_w^2 - (R_w - D)^2] \sim (eB/c)R_w D$. More precisely, the previous derivation[14] obtained the average change in canonical angular momentum $\langle \Delta P_\theta \rangle = (2/\pi)(eB/c)R_w D$.

Balancing the rate of change of the mode angular momentum against the rate of change of halo particle angular momentum yields the equation

$$\frac{d}{dt} N \frac{eB}{2c} D^2 + \left| \frac{dN}{dt} \right| \langle \Delta P_\theta \rangle = 0, \tag{1}$$

where $|dN/dt|$ is the rate per unit length at which halo particles pass through the resonance to the wall. Substituting for $\langle \Delta P_\theta \rangle$ yields the damping rate equation

$$\frac{dD}{dt} = -\frac{2}{\pi} \frac{1}{N} \left| \frac{dN}{dt} \right| R_w = -\gamma, \tag{2}$$

with a solution of linear algebraic damping $D(t) = D(0) - \gamma t$.

This simple result captures the experimental observations that the mode amplitude decays as a linear function of time and that the magnitude of the damping rate is proportional to the flux of halo particles through the resonant layer. The predicted magnitude of the damping rate is about half the measured rate.

Although this simple derivation has the advantage of brevity, it leaves questions unanswered. For example, given that the resonant particles cause mode damping, do they also

cause a mode frequency shift? Also, why focus exclusively on the thin ribbon of electrons beyond the critical contour, when there are many more resonant electrons? Is it really true that the mode transfers zero net angular angular momentum to these other resonant electrons?

A conceptual issue is the use of angular momentum balance. In fact, the total angular momentum for the plasma core and halo is not conserved. Transport continually changes the angular momentum of the halo particles as these electrons move out radially.

Also, the simple theory is implicitly based on a zero-diffusion model; the transport is assumed to be due exclusively to mobility. Unfortunately, the zero-diffusion model leads to an infinite density gradient at the leading edge of the halo, and such a gradient cannot be maintained in the presence of even a small diffusion coefficient. For the experimental conditions, diffusion affects the orbits of all the particles deemed responsible for damping in the simple theory. Indeed the whole idea of well-defined orbits looses meaning in the face of such diffusion. The orbits are diffusively broadened.

What is needed is a new, more rigorous theory based on a solution of the coupled Poisson and transport equations. Such a theory talks about an evolving density, rather the particle orbits, and makes no assumption about conservation of angular momentum.

We note at the outset, however, despite the problems listed above, the damping rate given in Eq. (2) will survive in the new theory, provided that the diffusion coefficient is sufficiently small, as defined by inequalities given later. The simple theory needs a more rigorous backup, indeed is wrong in detail, but captures the essence of the physics. The new theory does predict a frequency shift

$$\Delta\omega = \frac{32}{3}\frac{ecD}{BR_w}n^{(0)}(R_1), \tag{3}$$

where $n^{(0)}(R_1)$ is the unperturbed density in the resonant region of the halo.

The new theory preserves an important simplification of the traditional linear theory for an $m = 1$ diocotron mode[7]. For any unperturbed density perturbation $n^{(0)}(r)$ that is monotonically decreasing in r and goes to zero for some $r > R_w$, the mode perturbation results from a uniform displacement D of the plasma column off the trap axis. The displaced column produces an image in the conducting wall, and in the linear limit (i.e. $D/R_w \ll 1$), the electric field from the image is uniform over the whole column, producing a uniform $\mathbf{E} \times \mathbf{B}$ drift of the whole column transverse to the displacement $\mathbf{D}$. This uniform motion of

ing column around the trap axis is the mode.

In the traditional theory, there are no resonant particles near the wall, but the theory presented here must include such particles. Moreover, the perturbed charge density of the resonant particles produces an electric field that acts back on the plasma core, and one might worry that this field would spoil the picture of uniform core displacement. However, that is not the case.

The resonant particles are well outside the plasma core, so the field from the resonant particles is a vacuum field in the region of the core. The dipole portion of this field is the portion that drives the mode resonantly, and a dipole vacuum field is uniform. Recall that a dipole vacuum potential can be written in the form

$$\delta\phi(r,\theta,t) = -\delta E_x(t) r\cos\bar{\theta} - \delta E_y(t) r\sin\bar{\theta}, \tag{4}$$

where $\delta E_x(t)$ is the uniform field along the direction $\bar{\theta} = 0$ and $\delta E_y(t)$ is the uniform field along $\bar{\theta} = \pi/2$. We assume that the halo density is small, so the uniform field $\delta E_x(t)\hat{x} + \delta E_y\hat{y}$ is a small increment to the uniform field from the image in the wall and produces only a small increment in the uniform drift velocity of the core. Thus, the core perturbation is still a uniform displacement.

In Section II, the damping rate $\dot{D}$ and the frequency shift $\Delta\omega$ are obtained as Green's function integrals over the perturbed charge density in the resonant region. To obtain these integral expressions, the perturbed charge density of the core is taken to be of the form arising from a uniform displacement.

The integral expressions can be rewritten in the form

$$\dot{D} = \frac{c}{B}\delta E_y(t), D\Delta\omega = -\frac{c}{B}\delta E_x(t), \tag{5}$$

which yields a simple physical interpretation. The component of the uniform field from the resonant particles that is transverse to the displacement (δE_y) cause an $\mathbf{E}\times\mathbf{B}$ drift motion of the core back toward the trap axis, that is, a damping of the mode. Likewise, the component of the field along the displacement (δE_x) causes an increment to the $\mathbf{E}\times\mathbf{B}$ drift velocity around the trap axis, that is, a mode frequency shift.

A second re-writing of the integral expression for $\dot{D}$ clarifies the issue of angular momentum conservation. The equation can be re-written as a statement that the torque exerted by the core on the resonant particles is equal and opposite to the torque exerted by the

resonant particles back on the core. Two opposing torques are equal and opposite even if a third torque (say, due to the transport) acts. The treatment based on Poisson's equation correctly, and automatically, focuses on torque balance, rather than angular momentum balance.

For the conditions of the experiment, we will see that the transport caused change in angular momentum of electrons being swept to the wall is small compared to the change caused by the mode field, so the angular momentum balance is approximately correct. Nevertheless, the calculation of the damping rate should at least start from a rigorous foundation based on torque balance.

To obtain explicit expressions for the damping rate and frequency shift, the transport equation must be solved for the halo density distribution in the resonant region and the result substituted into the Green's function integrals. As a first step, the transport equation is discussed and simplified in Section III.

Note that the halo evolution takes place in two stages. First the halo extends radially outward until it reaches to the wall. At the wall, the electrons are continuously absorbed, and a quasi-steady state density distribution is established. We calculate the damping rate and frequency shift for this density distribution.

Section IV obtains simple analytic expressions for the density distribution, damping rate and frequency shift by using an idealized transport model: zero diffusion coefficient and constant coefficient of mobility. The $\mathbf{E} \times \mathbf{B}$ drift flow and mobility flow are then both incompressible and can be incorporated in a Hamiltonian description of the electron orbits. This idealized model implicitly underlies the simple theory[14,15], but leads to an infinite density gradient at the leading edge of the halo, which is untenable.

Section V includes the effect of diffusive broadening at the leading edge gradient. For the conditions of the experiments, the broadening substantially modifies the density distribution and the orbits in the region that determines the damping rate, so one might expect that the answer for the damping rate would be substantially changed. However, the Green's function integral for the damping rate can be rewritten in an approximate form that involves only the flux entering the broadening layer, and this form again yields the zero-diffusion damping rate in Eq. (2). The approximation requires that the diffusion coefficient be sufficiently small, as will be specified by inequalities in Section V. Subject to these inequalities the frequency shift is also relatively unchanged.

Numerical solutions for the diffusively broadened density distribution are obtained in Appendix A and are used in the Green's function integral to obtain numerical results for the damping rate. The numerical results are in good agreement with the approximate analytic result of Section V.

Section VI obtains a perturbative correction to the damping rate to account for the slow time dependence in $D(t)$. This time dependence causes the contours themselves to move, and the corrected damping rate is proportional to the flux through the moving contour. For the conditions of the experiment the correction is small.

Finally, Section VII is a discussion on the general applicability of this flux-driven damping mechanism.

II. GREEN'S FUNCTION SOLUTION FOR THE MODE DAMPING RATE AND FREQUENCY SHIFT

In this section, we obtain expressions for the mode damping rate and frequency shift as Green's function integrals over the perturbed charge density in the resonant region of the halo. To complete the calculation and obtain explicit expressions for the damping rate and frequency shift, one must solve for the perturbed charge density in the resonant region and substitute into the Green's function integrals. This second part of the calculation is deferred to later sections.

The linear $m = 1$ diocotron mode has the happy property[1,7,18] that the self-consistent density perturbation, mode potential and mode frequency are known analytically for any unperturbed density profile $n^{(0)}(r)$ that is monotonically decreasing in r and goes to zero for some $r < R_w$. The self-consistent density perturbation and mode potential are given by the expressions

$$\delta n(r,\theta,t) = -\frac{\partial n^{(0)}}{\partial r} D\cos(\theta - \omega_1 t - \alpha), \tag{6}$$

$$\delta\phi(r,\theta,t) = -\frac{rB}{c}[-\omega_1 + \omega_E(r)]D\cos[\theta - \omega_1 t - \alpha], \tag{7}$$

where $\omega_1 \equiv \omega_E(R_w)$ is the mode frequency. As mentioned above, the mode can be understood as a uniform displacement of the plasma column off the trap axis. From Eq. (6), one can see that the displacement is of magnitude D and in the instantaneous direction $\theta = \omega_1 t + \alpha$, where α is a phase shift. In Fig. (1), the angle in the wave frame is simply $\bar{\theta} = \theta - \omega_1 t - \alpha$.

The term $(rB/c)\omega_1 D\cos(\theta-\omega_1 t-\alpha)$ in the potential represents a uniform electric field due to the image of the displaced plasma in the conducting wall. Recall that the image is located far outside the wall in the linear theory limit where $D \ll R_w$. The uniform field produces a uniform $\mathbf{E}\times\mathbf{B}$ drift of the plasma as a whole. The direction of the image field is always along the direction of the instantaneous displacement, so the uniform drift velocity moves the plasma around the trap axis. The other term in the mode potential, $(-rB/c)\omega_E(r)D\cos(\theta-\omega_1 t-\alpha)$, simply accounts for a shift in the origin of the radial space charge field of the plasma column itself.

In this theory, there are no particles in the resonant region near the wall. However, here such particles must be included. As we will see, the mode potential acting on the resonant particles produces a perturbed resonant particle charge density, and this charge density produces a correction to the mode potential. This correction acts back on the particles in the non-resonant region causing a correction to the $\mathbf{E}\times\mathbf{B}$ drift motion. Nevertheless, we will postulate that the perturbed charge density in the non-resonant region continues to be of the form given by Eq. (6). Physically, the perturbation in the non-resonant region is still a uniform displacement.

Why is this the case? The resonant particles near the wall are all outside the non-resonant region, so the correction potential is a vacuum potential in the non-resonant region. Moreover, the dipole component of such potential represents a uniform electric field. Thus, the $\mathbf{E}\times\mathbf{B}$ drift velocity from this field is uniform over the whole non-resonant region and provides a small correction to the uniform drift velocity produced by the linear mode potential in Eq. (7). As we will see, the correction can be accounted for simply by allowing D and α in Eq. (6) to be time-dependent.

What is omitted in this description? First, the nonlinear orbits in the resonant region create density perturbations with azimuthal mode number greater than 1, and these harmonic perturbations produce fields in the non-resonant region that are not uniform. However, these harmonic fields do not drive the $m = 1$ diocotron mode resonantly, and the density perturbations produced are negligibly small.

Also neglected is an even smaller correction to the perturbed density in the non-resonant region that is caused by the transport. This correction is linear in mode amplitude and can lead to the kind of exponential damping or growth discussed earlier by Davidson and Chao[7]. We neglect this effect and focus on the interaction of the mode with resonant particles. This

ance is motivated by the experimental observation that the damping begins only when the halo particles reach the resonant region. The present theory is complementary to the earlier theory of Davidson and Chao[7].

The $m = 1$ Fourier components of the potential and density are related through the Green's function solution[9]

$$\delta\phi_1(r,t) = -4\pi e \int_0^{R_w} 2\pi r' dr' G_1(r|r')\delta n_1(r',t), \tag{8}$$

where

$$G_1(r|r') = \frac{1}{4\pi}\begin{cases} \dfrac{r}{r'}\left(\dfrac{r'^2}{R_w^2} - 1\right) & r < r' \\ \dfrac{r'}{r}\left(\dfrac{r^2}{R_w^2} - 1\right) & r' < r \end{cases} \tag{9}$$

is the Green's function and

$$\delta\phi_1(r,t) = \int_0^{2\pi} \frac{d\theta}{2\pi} e^{-i\theta}\delta\phi(r,\theta,t) \tag{10}$$

$$\delta n_1(r,t) = \int_0^{2\pi} \frac{d\theta}{2\pi} e^{-i\theta}\delta n(r,\theta,t) \tag{11}$$

are the Fourier components of the perturbed potential and density. Note that the Green's function satisfies the required boundary condition $G_1(R_w|r') = 0$. Also, note that Eq. (8) is valid whether or not linear theory can be used to find the density perturbation.

We postulate that the perturbed density can be written as

$$\delta n(r,\theta,t) = -D\cos(\theta - \omega_1 t - \alpha)\frac{\partial n^{(0)}}{\partial r}\mathcal{U}(R_1 - r) + \delta n'(r,\theta,t), \tag{12}$$

where $\mathcal{U}(R_1 - r)$ is a step-function and R_1 is the outer limit of the non-resonant region, that is, the region where linear theory may be used. The quantity $\delta n'(r,\theta,t)$ is the perturbed charge density in the resonant region (i.e., for $R_1 < r < R_w$). The postulated functional form for the non-resonant region ($r < R_1$) assumes that the perturbation is still a uniform displacement, even when the field from the resonant particles is taken into account, as explained in earlier.

Substituting Eq. (12) into Eq. (8) yields the relation

$$\delta\phi_1(r,t) = 4\pi e\frac{D}{2}e^{-i\omega_1 t - i\alpha}\int_0^{R_1} 2\pi r' dr' G_1(r|r')\frac{\partial n^{(0)}}{\partial r'} - 4\pi e\int_{R_1}^{R_w} 2\pi r' dr' G_1(r|r')\delta n_1'(r,t), \tag{13}$$

where

$$\delta n_1'(r,t) = \int_0^{2\pi}\frac{d\theta}{2\pi}\delta n'(r',\theta,t)e^{-i\theta} \tag{14}$$

is the Fourier component of $\delta n'(r,\theta,t)$. In evaluating the Green's function integrals, one must be careful to use the correct form of $G_1(r|r')$ depending on whether $r > r'$ or $r < r'$.

For the non-resonant region $r < R_1$, the Green's function integral in the first term yields the result

$$4\pi e\int_0^{R_1} 2\pi r'dr'G_1(r|r')\frac{\partial n^{(0)}}{\partial r'} = 4\pi e\left[\int_0^{r} 2\pi r'dr'G_1(r|r')\frac{\partial n^{(0)}}{\partial r'} + \int_r^{R_1} 2\pi r'dr'G_1(r|r')\frac{\partial n^{(0)}}{\partial r'}\right]$$
$$= 2er\left[\frac{N(r)}{r^2} - \frac{N(R_1)+\pi n^{(0)}(R_1)(R_w^2-R_1^2)}{R_w^2}\right], \tag{15}$$

where both integrals on the Right Hand Side have been integrated by parts and $N(r) \equiv \int_0^r 2\pi r'dr'n^{(0)}(r')$. For the resonant region $R_1 < r < R_w$, the Green's function integral in the first term yields the result

$$4\pi e\int_0^{R_1} 2\pi r'dr'G_1(r|r')\frac{\partial n^{(0)}}{\partial r'} = -2er\left(\frac{1}{R_w^2}-\frac{1}{r^2}\right)[N(R_1)-\pi R_1^2 n^{(0)}(R_1)], \tag{16}$$

where again integration by parts has been used.

We will need the potential in the resonant region later; here we focus on the potential in the non-resonant region, where Eq. (13) reduces to the form

$$\frac{c}{B}\delta\phi_1(r,t)e^{i\omega_1 t+i\alpha} = [\omega_1-\omega_E(r)]\frac{D}{2}r - \frac{4\pi ec}{B}\int_{R_1}^{R_w} 2\pi r'dr'G_1(r|r')\delta n_1'(r',t)e^{i\omega_1 t+i\alpha}. \tag{17}$$

Here, $\omega_E(r) = -2ecN(r)/Br^2$ is the rotation frequency, and ω_1 is given by $\omega_E(R_w)$, assuming that the density takes the constant value $n^{(0)}(R_1)$ in the resonant region $R_1 < r < R_w$. Note that the first term on the Right Hand Side of Eq. (17) has the same form as the coefficient of $\cos(\theta-\omega_1 t-\alpha)$ in Eq. (7) for the linear diocotron mode.

We will see that the density is not in fact constant in the resonant region; particles are excluded from the closed cat's eye orbits, and the frequency shift $\Delta\omega$ accounts for this fact.

The linearized the continuity equation[1] in the non-resonant region takes the form

$$\left[\frac{\partial}{\partial t}+i\omega_E(r)\right]\delta n_1(r,t) = \frac{ic}{Br}\delta\phi_1(r,t)\frac{\partial n^{(0)}}{\partial r}, \tag{18}$$

where a small correction to $\delta n_1(r,t)$ due to transport has been neglected.

Solving for $\delta\phi_1(r,t)$ in Eq. (17) and substituting into Eq. (18) yields the relation

$$re^{i\omega_1 t+i\alpha}\left[\frac{1}{i}\frac{\partial}{\partial t}+\omega_E(r)\right]\frac{\delta n_1(r,t)}{\partial n^{(0)}/\partial r}$$
$$= -[\omega_E(r)-\omega_1]\frac{D}{2}r - \frac{4\pi ec}{B}\int_0^{R_w} 2\pi r'dr'G_1(r|r')\delta n_1'(r',t)e^{i\omega_1 t+i\alpha}. \tag{19}$$

For a self-consistent solution, this equation must be satisfied when the non-resonant density perturbation postulated as the first term in Eq. (12) is substituted for $\delta n(r,t)$. Substituting and carrying out the time derivatives yield the equation

$$\begin{aligned} &-\frac{r}{2}\left\{\frac{1}{i}\frac{\partial D}{\partial t}-\frac{\partial \alpha}{\partial t}D+[\omega_E(r)-\omega_1]D\right\} \\ &=-[\omega_E(r)-\omega_1]\frac{D}{2}r-\frac{4\pi ec}{B}\int_0^{R_w}2\pi r'dr'G_1(r|r')\delta n'_1(r',t)e^{i\omega_1 t+i\alpha}. \end{aligned} \tag{20}$$

The two terms in square brackets cancel, leaving the result

$$-i\frac{\partial D}{\partial t}-\frac{\partial \alpha}{\partial t}D=\frac{8\pi ec}{Br}\int_{R_1}^{R_w}2\pi r'dr'G_1(r|r')\delta n'_1(r',t)e^{i\omega_1 t+i\alpha}. \tag{21}$$

In the non-resonant region ($r<R_1$), the upper form for the Green's function in Eq. (9) must be used, and this form is proportional to r. Thus, the r-dependence on the Right Hand Side of Eq. (21) cancels. When $D\partial\alpha/\partial t$ and $i\partial D/\partial t$ are chosen to match the real and imaginary time-dependence of the Right Hand Side, we have a self-consistent solution.

Using Eq. (14) and taking the real and imaginary parts of Eq. (21) yields the desired integral expressions for the damping rate and frequency shift

$$\frac{\partial D}{\partial t}=\frac{8\pi ec}{Br}\int_{R_1}^{R_w}r'dr'\int_0^{2\pi}d\theta G_1(r|r')\delta n'(r',\theta,t)\sin[\theta-\omega t-\alpha], \tag{22}$$

$$D\frac{\partial \alpha}{\partial t}=D\Delta\omega=-\frac{8\pi ec}{Br}\int_{R_1}^{R_w}r'dr'\int_0^{2\pi}d\theta G_1(r|r')\delta n'(r',\theta,t)\cos[\theta-\omega t-\alpha], \tag{23}$$

where $\Delta\omega\equiv\partial\alpha/\partial t$ is the frequency shift.

The argument of the sine and cosine functions in Eqs. (22) and (23) [i.e., $\bar{\theta}=\theta-\omega_1 t-\alpha$] is the angle measured in the instantaneous rotating frame of the wave, and the $\bar{\theta}$-integrals in these equations are simply the dipole Fourier components of $\delta n'(r,\theta,t)$ evaluated in the rotating frame. In subsequent sections, we will evaluate $\delta n'$ in this rotating frame.

A simple interpretation of Eqs. (22) and (23) provides a more mechanistic explanation of the damping and frequency shift. The interpretation starts from the observation that the Left Hand Side of the equations [i.e., $\partial D/\partial t$ and $\Delta\omega D$] both have the dimensions of velocity. As mentioned above, the charge density $e\delta n'(r,\theta,t)$ is zero for $r<R_1$, so the corresponding dipole potential produced in the region $r<R_1$ is of the vacuum form

$$\delta\phi'(r,\bar{\theta},t)=-r\delta E_x\cos\bar{\theta}-r\delta E_y\sin\bar{\theta}, \tag{24}$$

where δE_x and δE_y are independent of $\bar{\theta}$ and r. The Right Hand Sides of Eqs. (22) and (23) are simply expressions for $(c/B)\delta E_y$ and $-(c/B)\delta E_x$ respectively. Thus, Eq. (22) is simply a statement that the field δE_y, from the resonant particle charge density, produces an $\mathbf{E}\times\mathbf{B}$ drift motion of the plasma along the direction of instantaneous displacement $\mathbf{D}$, that is, a growth or damping of the displacement depending on the sign of δE_y. Likewise, Eqs. (23) is a statement that δE_x causes an $\mathbf{E}\times\mathbf{B}$ drift increment to the velocity of the plasma transverse to $\mathbf{D}$, and such an increment causes a frequency shift in the rate of rotation of the plasma around the trap axis, that is, an increment in the mode frequency.

Finally, how does the Green's function solution clarify the issues associated with the angular momentum balance argument[14,15]? Let $e\delta n_a(r,\bar{\theta})$ and $e\delta n_b(r,\bar{\theta})$ be two perturbed charge densities in a Penning trap. The torque exerted on $e\delta n_a(r,\bar{\theta})$ by the field from $e\delta n_b(r,\bar{\theta})$ is given by the integral

$$\tau_{a,b} = -e^2\int_0^{R_w} r'dr'\int_0^{2\pi} d\bar{\theta}'\int_0^{R_w} rdr\int_0^{2\pi} d\bar{\theta}\left\{\frac{1}{r}\left[\frac{\partial}{\partial\bar{\theta}}G(r,\bar{\theta},r',\bar{\theta}')\right]\cdot r\delta n_a(r,\bar{\theta})\delta n_b(r',\bar{\theta}')\right\}. \tag{25}$$

Because the trap has cylindrical symmetry, the Green's function has the functional form $G(r,\bar{\theta},r',\bar{\theta}') = G(r,r',\bar{\theta}-\bar{\theta}')$. Thus the opposing torques are equal and opposite [i.e., $\tau_{a,b}+\tau_{b,a}=0$], even if a third torque, such as that due to transport, acts.

Eq. (22) for the damping rate is equivalent to such a statement of torque balance. Let $\delta n_a(r,\bar{\theta})$ be the perturbed charge density of the non-resonant region [i.e., $-D\partial n^{(0)}/\partial r\cos\bar{\theta}$], and let $\delta n_b(r,\bar{\theta})$ be the dipole component of the perturbed charge density of the resonant region [i.e., the dipole component of $\delta n'(r,\bar{\theta})$]. The torque $\tau_{a,b}$ is given by the integral

$$\tau_{a,b} = \int_0^{R_1} rdr\int_0^{2\pi} d\bar{\theta}(-D\frac{\partial n^{(0)}}{\partial r}\cos\bar{\theta})\left(-\frac{e}{r}\frac{\partial\delta\phi_b}{\partial\bar{\theta}}\right)r. \tag{26}$$

Using orthogonality of the sinusoidal functions in the harmonic expansion of $\delta\phi_b(r,\bar{\theta})$, the $\bar{\theta}$-integral in Eq. (26) picks out the term $-rE_y\sin\bar{\theta}$ in the dipole portion of $\delta\phi_b(r,\bar{\theta})$, as given by Eq. (24), yielding the result

$$\begin{aligned}\tau_{a,b} &= -\pi DeE_y\int_0^{R_1} r^2dr\frac{\partial n^{(0)}}{\partial r}\\ &= -\pi D\frac{\partial D}{\partial t}\frac{eB}{c}\int_0^{R_1} r^2dr\frac{\partial n^{(0)}}{\partial r}.\end{aligned} \tag{27}$$

Multiplying Eq. (22) by $-\pi D(eB/c)r^2\partial n^{(0)}/\partial r$ and integrating over dr from $r=0$ to

$r = R_1$ yields the equation

$$\tau_{a,b} = -8\pi^2 e^2 \int_{R_1}^{R_w} r'dr' \int_0^{2\pi} d\bar{\theta}\delta n_b(r',\bar{\theta}) \int_0^{R_1} rdrG_1(r|r')\frac{\partial n^{(0)}}{\partial r} D\sin\bar{\theta}, \tag{28}$$

where $\delta n_b(r',\bar{\theta})$ has been substituted for $\delta n'(r',\bar{\theta})$. The potential $\delta\phi_a(r',\bar{\theta})$ is given by the expression

$$\delta\phi_a(r',\bar{\theta}) = -4\pi e \int_0^{R_1} 2\pi rdrG_1(r',r)[-D\frac{\partial n^{(0)}}{\partial r}\cos\bar{\theta}], \tag{29}$$

where $r' > R_1 \geq r$. Using the relation $G_1(r',r) = G_1(r,r')$ for $r' > r$ yields the result

$$\delta\phi_a(r',\bar{\theta}) = 8\pi^2 eD \int_0^{R_1} rdrG_1(r,r')\frac{\partial n^{(0)}}{\partial r}\cos\bar{\theta}, \tag{30}$$

so Eq. (26) can be rewritten as the result

$$\tau_{a,b} = -\int_{R_1}^{R_w} r'dr' \int_0^{2\pi} d\bar{\theta}\delta n_b(r',\bar{\theta})\left(-\frac{e}{r}\frac{\partial\delta\phi_a}{\partial\bar{\theta}}\right)r = -\tau_{b,a}. \tag{31}$$

III. TRANSPORT EQUATION

The particles move under the combined influence of an $\mathbf{E}\times\mathbf{B}$ drift flow and a radial transport flow, so the density evolves according to the equation

$$\frac{\partial n}{\partial t} + \frac{c}{B}\hat{z}\times\nabla_\perp\phi\cdot\nabla_\perp n + \frac{1}{r}\frac{\partial}{\partial r}r\Gamma_r(r) = 0, \tag{32}$$

where $\phi(r,\theta,t)$ is the electric potential and $\Gamma_r(r)$ is the radial transport flux.

We employ a Hamiltonian description of the drift dynamics, where $H(\theta,P_\theta,t) = e\phi[r(P_\theta),\theta,t]$ is the drift Hamiltonian and $(\theta, P_\theta = eBr^2/2c)$ are a canonically conjugate coordinate and momentum pair[17,19,20]. One can easily check that the Hamilton's equations of motion[21] are the same as the $\mathbf{E}\times\mathbf{B}$ drift equations in a uniform magnetic field $\mathbf{B} = B\hat{z}$. The Left Hand Side of Eq. (32) then can be written in the form

$$\frac{\partial n}{\partial t} + \frac{c}{B}\hat{z}\times\nabla_\perp\phi\cdot\nabla_\perp n = \frac{\partial n}{\partial t} + [n,H], \tag{33}$$

where $[n,H]$ is a Poisson bracket[22].

The transport is understood to be due to small static field asymmetries[23], which exert an azimuthal drag force on the rotating plasma, causing a radially outward drift motion. In the experiments[14], the transport flux is varied (i.e., increased) by applying additional field asymmetries.

On general grounds, the flux is expected to be of the Fick's law form[24]

$$\Gamma_r = -\mu \frac{\partial \phi_0}{\partial r} n - \mathcal{D} \frac{\partial n}{\partial r}, \tag{34}$$

where the coefficient of mobility μ and the diffusion coefficient $\mathcal{D}$ satisfy the Einstein relation, $\mu = e\mathcal{D}/T < 0$. Here, $-\partial\phi_0/\partial r$ is the unperturbed radial electric field and T is the temperature in the halo region. The Fick's law form follows from the requirement that the flux vanish for a thermal equilibrium density profile, $n(r) = n_0 \exp[-e\phi_0(r)/T]$.

By changing variables from (r, θ, t) to (θ, P_θ, t), Eq. (32) takes the form

$$\frac{\partial n}{\partial t} + [n, H] = \frac{\partial}{\partial P_\theta}\left[-\dot{P}_\theta|_T n + \tilde{\mathcal{D}} \frac{\partial n}{\partial P_\theta}\right], \tag{35}$$

where

$$\dot{P}_\theta|_T = -\mu \frac{eB}{c} r \frac{\partial \phi_0}{\partial r}, \tilde{\mathcal{D}} = -\frac{\dot{P}_\theta|_T P_\theta \cdot 2T}{re\partial\phi_0/\partial r}. \tag{36}$$

Here $\dot{P}_\theta|_T$ is the rate at which mobility changes the value of P_θ of a particle. Note that $\tilde{\mathcal{D}}$ is proportional to $\dot{P}_\theta|_T$ and that $\dot{P}_\theta|_T < 0$ and $\tilde{\mathcal{D}} > 0$ since $e\partial\phi/\partial r$ is negative. We will need the transport equation in the resonant region where to a good approximation $er\partial\phi_0/\partial r$ is approximately $-2e^2N$ and P_θ is approximately $P_w \equiv eBR_w^2/2c$, where N is the number of particles per unit length. Thus the transport coefficients takes the simple form

$$\dot{P}_\theta|_T = \mu \frac{B}{c} \cdot 2e^2 N, \tilde{\mathcal{D}} = \dot{P}_\theta|_T P_w \frac{T}{Ne^2}. \tag{37}$$

For the experimental conditions, the factor T/Ne^2 in the diffusion coefficient is small (i.e., $T/Ne^2 \sim 10^{-2}$), so the transport is dominated by mobility everywhere except at the leading edge of the halo where a large density gradient enhances the effect of diffusion.

As noted in the last section, it is convenient to work in the rotating frame of the wave. The generating function[22]

$$F(\theta, \bar{P}_\theta, t) = \bar{P}_\theta[\theta - \omega_1 - \alpha(t)] \tag{38}$$

yields a canonical transformation to this frame, with the new coordinate and momentum

$$\bar{\theta} = \theta - \omega_1 t - \alpha(t), \bar{P}_\theta = P_\theta \tag{39}$$

and the new Hamiltonian

$$\bar{H} = H + \frac{\partial F}{\partial t} = H - (\omega_1 + \Delta\omega) P_\theta, \tag{40}$$

This manuscript was accepted by Phys. Plasmas. Click here to see the version of record.

where $\Delta\omega = \dot{\alpha}$. Since $\bar{P}_\theta$ and P_θ are equal, we continue to use P_θ in the new Hamiltonian. To work in the rotating frame, one need to only replace H by $\bar{H}$ in Eq. (35); the Right Hand Side of the equation need not be changed since the radial flux is the same in both frames.

Since the transport flow is slow compared to the $\mathbf{E}\times\mathbf{B}$ drift flow, the halo particles very nearly follow curves of constant $\bar{H}$. Thus, changing independent variables from $(\bar{\theta}, P_\theta, t)$ to $(\bar{\theta}, \bar{H}, t)$ in Eq. (35) is useful. The result is the transport equation

$$\left.\frac{\partial n}{\partial t}\right|_{\bar{\theta},\bar{H}} + \left.\frac{\partial n}{\partial \bar{H}}\right|_{\bar{\theta},t}\left.\frac{\partial \bar{H}}{\partial t}\right|_{\bar{\theta},P_\theta} + \left.\frac{\partial n}{\partial \bar{\theta}}\right|_{\bar{H},t}\left.\frac{\partial \bar{H}}{\partial P_\theta}\right|_{\bar{\theta},t} = \left.\frac{\partial \bar{H}}{\partial P_\theta}\right|_{\bar{\theta},t}\frac{\partial}{\partial \bar{H}}[-\dot{P}_\theta|_T n + \tilde{\mathcal{D}}\left.\frac{\partial \bar{H}}{\partial P_\theta}\right|_{\bar{\theta},t}\left.\frac{\partial n}{\partial \bar{H}}\right|_{\bar{\theta},t}]. \quad (41)$$

To complete the description of the transport equation, the Hamiltonian $\bar{H}(\bar{\theta}, P_\theta, t)$ is needed. Formally, the Hamiltonian is given by the expression

$$\bar{H} = e\phi_0[r(P_\theta)] + e\delta\phi[r(P_\theta), \bar{\theta}] - (\omega_1 + \Delta\omega)P_\theta, \quad (42)$$

where $\phi_0(r)$ is the unperturbed potential and $\delta\phi(r,\bar{\theta})$ is the perturbation caused by the mode.

As mentioned in the introduction, the transport equation can be simplified by using the smallness of the halo density n_h in the resonant region. Our goal is to calculate the damping rate and frequency shift to first order in this small quantity. From Eqs. (22) and (23) one can see that the integral expressions for the damping rate and frequency shift are already first order small in n_h. Thus, the functional form of the perturbed halo density in the resonant region need only be accurate to zero order in n_h. Likewise, the transport equation, which determines the functional form, need only be accurate to zero order in the halo density.

Of course, n_h is not a dimensionless parameter on which to base a proper ordering scheme. The dimensionless ordering parameter is $N_h/N \equiv (n_h\pi R_w^2)/N$, which has the value 0.1 for typical experimental conditions. As we will see, even the largest of the neglected terms is down by this dimensionless factor.

Let us start by simplifying the Hamiltonian. In the resonant region, where the transport equation and Hamiltonian are needed, the dipole contribution to the perturbed potential is given by the expression

$$\delta\phi_1(r,t) = -erD[N(R_1) - \pi R_1^2 n^{(0)}(R_1)]\left(\frac{1}{R_w^2} - \frac{1}{r^2}\right)e^{-i\omega_1 t - i\alpha} - 4\pi e\int_{R_1}^{R_w} 2\pi r' dr' G_1(r|r')\delta n_1'(r',t), \quad (43)$$

where use has been made of Eqs. (13) and (16). The first term is the contribution to the dipole potential from the non-resonant region, and the second is the contribution from the

nonant region. Simple estimates show that the second term is smaller than the first term by a factor of N_h/N, so we neglect the second term. The higher harmonic contributions to the perturbed potential are comparably small and also are neglected. The constant square bracket in the first term can be replaced by N with a relative error that is down by a factor N_h/N. Finally, there is a small $\bar{\theta}$-independent contribution to the perturbed potential, which we also neglect. The radial electric field from this potential is smaller than that from the unperturbed potential $\phi_0(r)$ by a factor that is much smaller than N_h/N. Thus, the perturbed potential reduces to the simple form

$$\delta\phi(r,\bar{\theta}) = -2eNDr\left(\frac{1}{R_w^2} - \frac{1}{r^2}\right)\cos\bar{\theta}. \tag{44}$$

In the resonant region, the Hamiltonian can be simplified further by Taylor expansion with respect to P_θ about $P_\theta = P_w$. Setting $\phi_0(R_w) = 0$, using $\partial\phi_0/\partial r \simeq -2Ne/r$ near the wall and using the resonance condition $\omega_1 = \omega_E(R_w) = (c/BR_w)(\partial\phi_0/\partial r)|_{R_w}$ yield the expansion

$$\bar{H} = \frac{Ne^2}{2}\left\{\left(\frac{P_\theta - P_w}{P_w}\right)^2 - \frac{4D}{R_w}\left(\frac{P_\theta - P_w}{P_w}\right)\left[\cos\bar{\theta} + \frac{R_w P_w \Delta\omega}{2DNe^2}\right]\right\}, \tag{45}$$

where higher than second order terms in the small quantity $|P_\theta - P_w|/P_w \sim 4D/R_w$ have been dropped and the purely time-dependent term $\Delta\omega P_w$ has been added.

We will see that the second term in the square bracket is a constant of value $0.6(N_h/N_c)$. This term can be retained in the analysis, but for consistency (and simplicity) is dropped here yielding the reduced Hamiltonian

$$\bar{H} = \frac{Ne^2}{2}\left[\left(\frac{P_\theta - P_w}{P_w}\right)^2 - \left(\frac{P_\theta - P_w}{P_w}\right)\cdot\frac{4D}{R_w}\cos\bar{\theta}\right]. \tag{46}$$

The time dependence of the transport equation also can be simplified by using the smallness of N_h/N. In the introduction, we noted that the halo evolution can be divided into two stages. First the halo extends radially out to the wall. At the wall, particles are continuously absorbed and a quasi-steady state density distribution is established. We calculate the damping rate and frequency shift for this quasi-steady state density distribution.

The modifier "quasi" is used since the density continues to change slowly due to the slow damping, that is, due to the time dependence in $D(t)$, which enters the Hamiltonian. In Sections 4 and 5, we neglect this slow time dependence, that is, neglect the first two terms

This manuscript was accepted by Phys. Plasmas. Click here to see the version of record.

ing the Left Hand Side of Eq. (41), to obtain the simplified transport equation

$$\left.\frac{\partial n}{\partial \bar{\theta}}\right|_{\bar{H}} = \frac{\partial}{\partial \bar{H}}[-\dot{P}_\theta|_T n + \tilde{\mathcal{D}} \left.\frac{\partial \bar{H}}{\partial P_\theta}\right|_{\bar{\theta}} \left.\frac{\partial n}{\partial \bar{H}}\right|_{\bar{\theta}}]. \tag{47}$$

One expects the corrections due to the neglected time dependence to be small since $\dot{D}(t)$ is first order small in n_h. In Section 6, a perturbative treatment is used to show that the relative correction to the damping rate is approximately $\Delta\gamma/\gamma \simeq 2N_h/N$. The relative correction to the frequency shift is even smaller.

For plotting purposes, it is useful to re-write the reduced Hamiltonian in the scaled form

$$h = p^2 - p\cos\bar{\theta}, \tag{48}$$

where

$$p = \left(\frac{P_\theta - P_w}{P_w}\right)\left(\frac{R_w}{4D}\right), \tag{49}$$

$$h = \frac{2\bar{H}}{Ne^2}\left(\frac{R_w}{4D}\right)^2. \tag{50}$$

Likewise transport equation (47) takes the scaled form

$$\left.\frac{\partial n}{\partial \bar{\theta}}\right|_h = \frac{\partial}{\partial h}[\beta n - \delta \left.\frac{\partial h}{\partial p}\right|_{\bar{\theta}} \left.\frac{\partial n}{\partial h}\right|_{\bar{\theta}}]_{\bar{\theta}}, \tag{51}$$

where

$$\beta = -\frac{2\dot{P}_\theta|_T}{Ne^2}\left(\frac{R_w}{4D}\right)^2, \tag{52}$$

$$\delta = \beta\frac{T}{Ne^2}\left(\frac{R_w}{4D}\right). \tag{53}$$

To lowest order in the Taylor expansion, β and δ are treated as constant in the resonant region. Except for the smallest values of D accessed in the experiments, these constants are ordered as $\delta \ll \beta \ll 1$.

Fig. (2) shows a contour plot of $h(\bar{\theta}, p)$ in the resonant region near the wall. The ordinate of the plot ranges from $p = 0$, the location of the wall, to $p = -2$, which is enough of the $(\bar{\theta}, p)$ phase space to show the resonant region. Of course, the full phase space extends to much lower values of p where the plasma core is located.

The contours of constant $h(\bar{\theta}, p)$ are the trajectories that would be followed by a particle moving only under the $\mathbf{E}\times\mathbf{B}$ drift flow, and the arrows on the contours indicate the direction of the flow. There are open trajectories extending from $\bar{\theta} = 0$ to $\bar{\theta} = 2\pi$, closed trajectories,

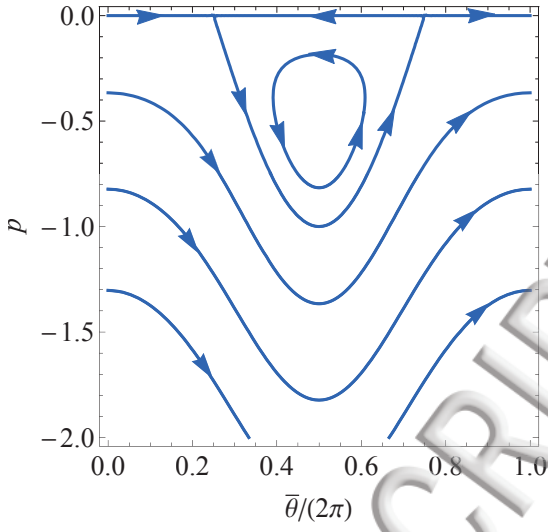

FIG. 2. Contours of $h(\bar{\theta}, p)$

and a separatrix between the two. The value of h is positive on the open trajectories, zero on the separatrix, and negative on the closed trajectories. The closed trajectories are the "cat's eye" trajectories.

Solving Eq. (48) yields a solution for the trajectories

$$p_{\pm} = \frac{\cos\bar{\theta} \pm \sqrt{\cos^2\bar{\theta} + 4h}}{2}, \tag{54}$$

where the minus sign is to be used for the open trajectories, on which $p(\bar{\theta})$ is a single-valued function of $\bar{\theta}$. Both the plus and minus signs are needed for the closed trajectories, where $p(\bar{\theta})$ is double-valued.

Adjacent to the wall, there is a thin scrape-off layer where guiding center drift theory fails, and particles (electrons) are absorbed by the wall. The scrape-off layer is at least as thick as a cyclotron radius, which is of order 10^{-4} cm for the experiments. However, other effects, such as misalignment of and ripples in the magnetic field, likely increase the thickness of the scrape-off layer. In this regard, note that the particles undergo rapid axial bounce motion and azimuthal drift motion relative to the wall, so any region of the wall where the scrape-off mechanism reaches out furthest sets the overall thickness of the scrape-off layer.

The scrape-off mechanism and the thickness of the scrape-off layer Δr are not known experimentally, but we believe that the thickness Δr is small compared to the mode amplitude D, for the range of amplitudes in the experiments. This condition is necessary for the damping rate and the frequency shift to be independent of thickness. Note that a physical

thickness Δr corresponds to a scaled momentum thickness $\Delta p = \Delta r/2D$.

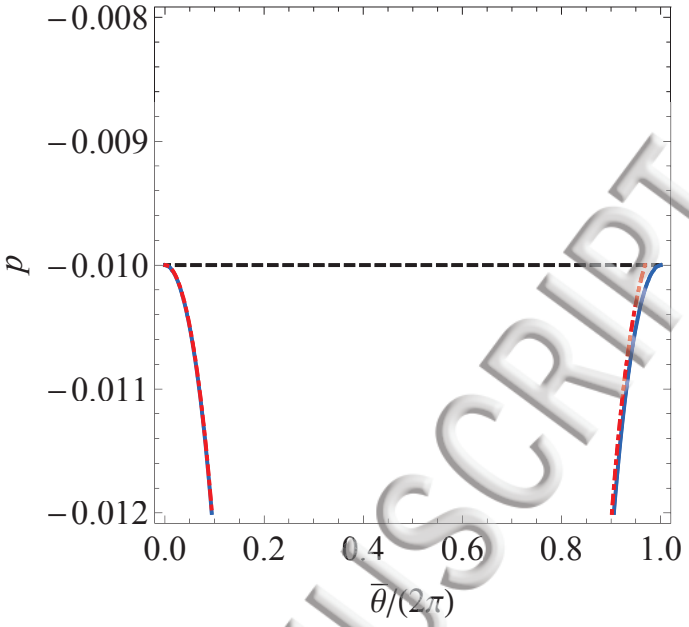

FIG. 3. Contours of $h = h_c$ (blue solid), $k = h_c$ (red dot-dashed) and the scrape-off layer (black dashed) in the $(\bar{\theta}, p)$ plane.

Fig. (3) shows a blow up of the phase space near the scrape-off layer, which for the sake of the figure is taken to have the thickness $\Delta p = 10^{-2}$. The lower edge of the scrape-off layer is shown as the black dashed line at $p = -\Delta p = -10^{-2}$. The solid blue contour is the critical contour, $h(\bar{\theta}, p) = h_c$, which just misses the scrape-off layer at $\bar{\theta} = 0$ and $\bar{\theta} = 2\pi$. Eq. (48) implies that the value of h on the critical contour is given by $h_c = (\Delta p)^2 + \Delta p \simeq \Delta p = 10^{-2}$. Also shown is a red dot-dashed curve that will be explained in the next section.

Fig. (4) shows the scrape-off layer and critical contour in $(\bar{\theta}, h)$-space. The solid blue horizontal line is the critical contour $h = h_c \simeq 10^{-2}$, and the black dashed curve is the lower edge of the scrape-off layer at $h = h(\bar{\theta}, -\Delta p) \simeq \Delta p(\cos\bar{\theta})$. Also shown is the red dot-dashed curve of Fig. (3).

For orientation, note that p increases upward in Fig. (3) and that h increases upward in Fig. (4). Thus, the core plasma is below the region shown in Fig. (3) and above the region in Fig. (4).

In the region $h > h_c$ of Fig. (4), the contours of constant h extend from $\bar{\theta} = 0$ to $\bar{\theta} = 2\pi$. Since the points $(\bar{\theta} = 0, h)$ and $(\bar{\theta} = 2\pi, h)$ are the same point physically, we require that $n(\bar{\theta} = 0, h) = n(\bar{\theta} = 2\pi, h)$ in the region $h > h_c$. In the region $0 < h < h_c$, the contours

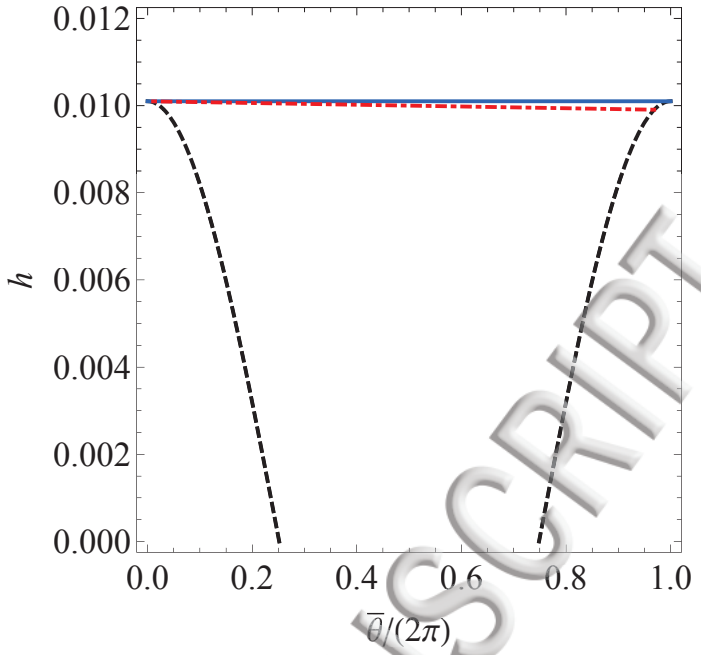

FIG. 4. Contours of $h = h_c$ (blue solid), $k = h_e$ (red dot-dashed) and the scrape-off layer (black dashed) in the $(\bar{\theta}, h)$ plane.

of constant h encounter the scrape-off layer before reaching $\bar{\theta} = 0$ or $\bar{\theta} = 2\pi$. The particle density within the scrape-off layer is taken to be zero. This implies that no particles emerge from the scrape-off layer and, when diffusion is taken into account, that the particle density at the surface of the scrape-off layer be zero. Otherwise, there would be an infinite density gradient at the surface, which is unsustainable in the face of diffusion.

IV. ZERO DIFFUSION MODEL

As was noted earlier, the scaled diffusion coefficient, δ, is small compared to the scaled mobility coefficient β. Motivated by this observation, the previous calculation[14,15] of the damping rate assumed the limit of zero diffusion.

A review of this simple model is instructive since it admits a trivial analytic solution for the steady state density profile. Happily, the model yields the same answer for the damping rate and frequency shift as a more realistic model that includes small but finite diffusion [see Section 5].

Setting $\delta = 0$ and treating β as a constant reduces transport equation (51) to the simple

from

$$\left.\frac{\partial n}{\partial \bar{\theta}}\right|_h - \beta \left.\frac{\partial n}{\partial h}\right|_{\bar{\theta}} = 0, \tag{55}$$

which immediately yields the solution

$$n(\bar{\theta}, h) = g[h + \beta\bar{\theta}]. \tag{56}$$

The flow is incompressible along trajectories of constant $k = h + \beta\bar{\theta}$.

To understand this result physically, note that constant β implies constant $\dot{P}_\theta|_T$, which in turn implies that the mobility flow is incompressible. The mobility flow can then be incorporated along with the incompressible $\mathbf{E} \times \mathbf{B}$ drift flow in a Hamiltonian description. One can easily check that the Hamiltonian

$$K(\bar{\theta}, P_\theta) = H(\bar{\theta}, P_\theta) - \dot{P}_\theta|_T \bar{\theta} \tag{57}$$

generates both the $\mathbf{E} \times \mathbf{B}$ drift flow and the mobility flow. Since we are neglecting any explicit time dependence in this Hamiltonian, it is a constant of motion, that is, particles flow along curves of constant K. The equation $k = h(\bar{\theta}, p) + \beta\bar{\theta}$ is simply the scaled version of Eq. (57). Since the Hamiltonian flow is incompressible, the density is constant along the contour of constant k.

The red dot-dashed curves in Figs. (3) and (4) are two views of the critical trajectory $k = h_c$, drawn for the value $\beta = 2 \times 10^{-4}$, which is characteristic of the experimental conditions. This trajectory just misses the scrape-off layer at $\bar{\theta} = 0$ but enters the scrape-off layer just to the left of $\bar{\theta} = 2\pi$.

For the region $h > h_c$, the periodic boundary condition $n(\bar{\theta} = 0, h) = n(\bar{\theta} = 2\pi, h)$ plus the solution in Eq. (56) implies the relation $n(\bar{\theta} = 0, h) = n(\bar{\theta} = 2\pi, h + 2\pi\beta)$. Thus, $n(\bar{\theta} = 0, h)$ must be constant in the region $h > h_c$. The possibility of a periodic component with the very short periodicity scale $\delta h \sim 2\pi\beta$ is ruled out by even small diffusion. This conclusion will be clarified in the next section.

Every point above the red dot-dashed contour in Fig. (4), that is, above the trajectory $k = h_c$, lies on a trajectory that emerges from the line interval ($\bar{\theta} = 0$, $h > h_c$), on which the density has a constant value. Thus, the density in the whole region above the red dot-dashed trajectory has this constant value. The density below the red dot-dashed trajectory is zero, because there the points lie on trajectories that emerge from the scrape-off layer. Thus, the

This manuscript was accepted by Phys. Plasmas. Click here to see the version of record.

density is given by the expression

$$n(\bar{\theta}, h) = n^{(0)}(R_1)\mathcal{U}[h - h_c + \beta\bar{\theta}], \tag{58}$$

where $\mathcal{U}(x)$ is a step-function, and we have identified the value of the constant density as $n^{(0)}(R_1)$, the density at the beginning of the resonant region.

Eqs. (22) and (23) for the damping rate and frequency shift can be re-written in the form

$$\frac{\partial D}{\partial t} = \frac{ecR_w}{B}\left(\frac{4D}{R_w}\right)^2 \int_0^{2\pi} d\bar{\theta} \sin\bar{\theta} \int_{p(R_1)}^{0} pdp \cdot n[\bar{\theta}, h(\bar{\theta}, p)], \tag{59}$$

$$D\Delta\omega = -\frac{ecR_w}{B}\left(\frac{4D}{R_w}\right)^2 \int_0^{2\pi} d\bar{\theta} \cos\bar{\theta} \int_{p(R_1)}^{0} pdp \cdot n[\bar{\theta}, h(\bar{\theta}, p)], \tag{60}$$

where the relations

$$r'dr' = 2DR_w dp \tag{61}$$

$$\frac{G_1(r|r')}{r} = \frac{1}{4\pi r'}\left(\frac{r'^2}{R_w^2} - 1\right) \simeq \frac{Dp}{\pi R_w^2} \tag{62}$$

have been used, and the Green's function has been Taylor expanded about $r' = R_w$ in the last step of Eq. (62).

Substituting Eq. (58) for the density and carrying out the p-integrals yields the expressions

$$\frac{\partial D}{\partial t} = \frac{ecR_w}{B}\left(\frac{4D}{R_w}\right)^2 n^{(0)}(R_1) \int_0^{2\pi} d\bar{\theta} \frac{\sin\bar{\theta}}{2} \{p_-^2[\bar{\theta}, h_c - \beta\bar{\theta}] - p^2(R_1)\}, \tag{63}$$

$$D\Delta\omega = -\frac{ecR_w}{B}\left(\frac{4D}{R_w}\right)^2 n^{(0)}(R_1) \int_0^{2\pi} d\bar{\theta} \frac{\cos\bar{\theta}}{2} \{p_-^2[\bar{\theta}, h_c - \beta\bar{\theta}] - p^2(R_1)\}, \tag{64}$$

where $p_-(\bar{\theta}, h)$ is given by Eq. (54) with the minus sign chosen.

In the curly brackets of both integrals, the constant term $p^2(R_1)$ integrates to zero. Using the smallness of β, the other term in the curly brackets may be Taylor expanded yielding the expression

$$p_-^2[\bar{\theta}, h_c - \beta\bar{\theta}] = p_-^2(\bar{\theta}, h_c) - 2p_-(\bar{\theta}, h_c)\left[\frac{\partial p_-}{\partial h}(\bar{\theta}, h_c)\right]\beta\bar{\theta}. \tag{65}$$

The first term in this Taylor expansion does not integrate to zero when substituted into Eq. (64) for the frequency shift, so the smaller, second term may be neglected, yielding the expression

$$D\Delta\omega = -\frac{ecR_w}{B}\left(\frac{4D}{R_w}\right)^2 n^{(0)}(R_1) \int_0^{2\pi} d\bar{\theta} \frac{\cos\bar{\theta}}{2} p_-^2(\bar{\theta}, h_c). \tag{66}$$

For $h_c \ll 1$, Eq. (54) implies that $p_-^2(\bar{\theta}, h_c)$ is approximately given by $\cos^2\bar{\theta}$ in the interval $\pi/2 < \bar{\theta} < 3\pi/2$ and is nearly zero elsewhere. Thus, Eq. (66) reduces to the result

$$\Delta\omega = -\frac{ecR_w}{BD}\left(\frac{4D}{R_w}\right)^2 n^{(0)}(R_1)\int_{\pi/2}^{3\pi/2} d\bar{\theta}\frac{\cos^3\bar{\theta}}{2}$$
$$= \frac{32}{3}\frac{ecn^{(0)}(R_1)}{B}\frac{D}{R_w}. \tag{67}$$

Eqs. (15) and (17) show that the frequency ω_1 has the value $\omega_E(R_w)$, assuming that the density has the constant value $n^{(0)}(R_1)$ in the resonant region $R_1 < r < R_w$. For the density solution given by Eq. (56), the density does not extend at the constant value $n^{(0)}(R_1)$ to the wall, but only to the dot-dashed trajectory in Figs. (3) and (4). The particles are excluded from the closed cat's eye orbits adjacent to the wall. The frequency shift accounts for this exclusion, yielding an effective exclusion length of $\Delta r = (8/3\pi)D$.

In progressing from Eq. (45) to Eq. (46), the quantity $(R_w P_w \Delta\omega)/(2DNe^2)$ was dropped, anticipating that it would be small compared to unity. Substituting for $\Delta\omega$ from Eq. (67) shows that the quantity is indeed small:

$$\frac{R_w P_w \Delta\omega}{2DNe^2} = \frac{8}{3}\frac{R_w^2 n^{(0)}(R_1)}{N} \simeq 0.06. \tag{68}$$

In Eq. (63) for the damping rate, the first term in Taylor expansion (65) integrates to zero, since $p_-^2(\bar{\theta}, h)$ is even in $\bar{\theta}$ about $\bar{\theta} = \pi$ and $\sin\bar{\theta}$ is odd. Thus, the integral is determined solely by the second term in the Taylor expansion and reduces to the form

$$\frac{\partial D}{\partial t} = -\frac{ecR_w}{B}\left(\frac{4D}{R_w}\right)^2 n^{(0)}(R_1)\int_0^{2\pi} d\bar{\theta}\sin\bar{\theta}\, p_-(\bar{\theta}, h_c)\left[\frac{\partial p_-}{\partial h}(\bar{\theta}, h_c)\right]\beta\bar{\theta}. \tag{69}$$

Eqs. (48) and (54) imply the relation

$$p_-(\bar{\theta}, h_c)\left[\frac{\partial p_-}{\partial h}(\bar{\theta}, h_c)\right] = \frac{-\cos\bar{\theta} + \sqrt{\cos^2\bar{\theta} + 4h}}{2\sqrt{\cos^2\bar{\theta} + 4h}}. \tag{70}$$

For $h = h_c \simeq \Delta p \ll 1$, the Right Hand Side has the approximate value 1 for $\pi/2 < \bar{\theta} < 3\pi/2$ and is nearly zero elsewhere. Thus, Eq. (69) yields the result

$$\frac{\partial D}{\partial t} = -\frac{ecR_w}{B}\left(\frac{4D}{R_w}\right)^2 n^{(0)}(R_1)\int_{\pi/2}^{3\pi/2} d\bar{\theta}\sin\bar{\theta}\beta\bar{\theta}$$
$$= +\frac{ecR_w}{B}\left(\frac{4D}{R_w}\right)^2 n^{(0)}(R_1)\cdot 2\beta. \tag{71}$$

By using Eq. (52) and the relation

$$n^{(0)}(R_1)\dot{P}_\theta|_T = \frac{eB}{2\pi c}\left|\frac{dN}{dt}\right|, \tag{72}$$

Eq. (71) reduces to the previous result for the damping rate[14,15], as given by Eq. (2).

The second term in Taylor expansion (65) represents the particle density in the region between the solid and the dot-dashed curves of Figs. (3) and (4) [i.e., between $h = h_c$ and $k = h_c$], so the damping rate is determined exclusively by particles in this region. From Fig. (3), one can see that these are particles that are being swept around the cat's eye orbits to the scrape-off layer and wall.

The previous calculation[14,15] guessed that the wave torque is dominantly applied to these particles, approximated that torque by the the rate of change of angular momentum of the particles, and evaluated the change in angular momentum using the zero diffusion orbits discussed in this section.

A particle enters the region between the solid and the dot-dashed curves when mobility transports the particle through the contour $h = h_c$. The rate at which particles flow through this contour between $\bar{\theta}$ and $\bar{\theta} + d\bar{\theta}$ is proportional to $\beta n d\bar{\theta}$. Since βn is constant, the flux is uniform in $\bar{\theta}$. Since all of the particles enter the scrape-off layer at $p = -\Delta p$, the average change in angular momentum for the particles is simply

$$\langle \Delta P_\theta \rangle = \int_0^{2\pi} \frac{d\bar{\theta}}{2\pi} P_w \frac{4D}{R_w} [-\Delta p - p_-(\bar{\theta}, h_c)]. \tag{73}$$

Using the inequality $h_c \simeq \Delta p \ll 1$ and Eq. (54) yields the result

$$\Delta P_\theta \simeq -\frac{eBR_w}{\pi c} \int_{\pi/2}^{3\pi/2} d\bar{\theta} \cos\bar{\theta} = \frac{2}{\pi} \frac{eBR_w D}{c}, \tag{74}$$

which is the result quoted in the introduction. The rate of change of angular momentum was then written as $|dN/dt|\langle \Delta P_\theta \rangle$ and used as the torque in the torque balance equation to obtain the damping rate in Eq. (2).

Since this previous calculation approximates the wave torque on the halo particles by the rate of change of halo particle angular momentum, omitting the torque due to the transport, one may ask why the present and previous calculations agree. The answer is that the torque exerted on a particle while it is being swept around the cat's eye orbit is small, of order β. Also, the quantity $|dN/dt|$ is first order in β, so the correction would be of order β^2. Likewise in the Taylor expansion of Eq. (65) only the term first order in β was retained. Thus, the two calculations are accurate only to order β, and differences would appear in order β^2.

IV. DIFFUSIVE BROADENING

An obvious criticism of the zero-diffusion model is that it leads to an infinite density gradient at the leading edge of the halo [i.e. at $k = h_c$], and even a small diffusion gradient must broaden such a gradient. This broadening is worrisome since the damping rate in the zero diffusion model is determined by a thin ribbon of particles at the leading edge of the halo. Moreover, for the conditions of the experiments, the diffusively broadened layer is much wider than the ribbon. Nevertheless, we will find that the answer for the damping rate is not changed significantly, provided the diffusive broadening is not too large, as will be specified by constraints on the size of the diffusion coefficient.

Numerical solutions of transport equation (51) are obtained in Appendix A. The boundary conditions imposed on the solution are that $n(\bar{\theta}, h)$ approaches the constant value $n^{(0)}(R_1)$ for sufficiently large h, that $n(\bar{\theta} = 0, h) = n(\bar{\theta} = 2\pi, h)$ for $h > h_c$ and that $n(\bar{\theta}, h)$ be zero at the surface of the scrape-off layer. The dynamics itself will prevent particles from reaching the contour $h = 0$.

Fig. (5) shows a contour plot of the relative density $n(\bar{\theta}, h)/n^{(0)}(R_1)$ obtained for the transport coefficient values $\beta = 10^{-5}$ and $\delta = 4 \times 10^{-7}$, which are characteristic values for the experiments. Only the relative density need be specified since the transport equation is linear and the boundary conditions are homogeneous. The critical contour $h = h_c$ is again drawn as a solid blue line. Likewise, the red dot-dashed line is the trajectory $k = h_c$, and the dashed black curves are the surface of the scrape-off layer. Clearly the thin ribbon between the solid blue line and the dot-dashed red line is very narrow compared to the width of the diffusive broadening.

In order to show the full range of diffusive broadening, the range of h values shown in Fig. (6) is larger than that in Fig. (5). The upper dotted blue curve in Fig. (6) shows the h-scale length for diffusive broadening in the region $h > h_c$, and the lower dotted blue curve shows the scale length in the region $0 < h < h_c$. The diffusive broadening scales are different in the two regions, since the boundary conditions of the transport equation (51) are different in the two regions.

To estimate the h-scale length for diffusive broadening in the region $h > h_c$, we use a perturbation expansion of Eq. (51) based on the smallness of β and δ. Substituting the expansion $n(\bar{\theta}, h) = n^{(0)}(\bar{\theta}, h) + n^{(1)}(\bar{\theta}, h)$, where $n^{(1)}/n^{(0)}$ is first order in β and δ, yields the

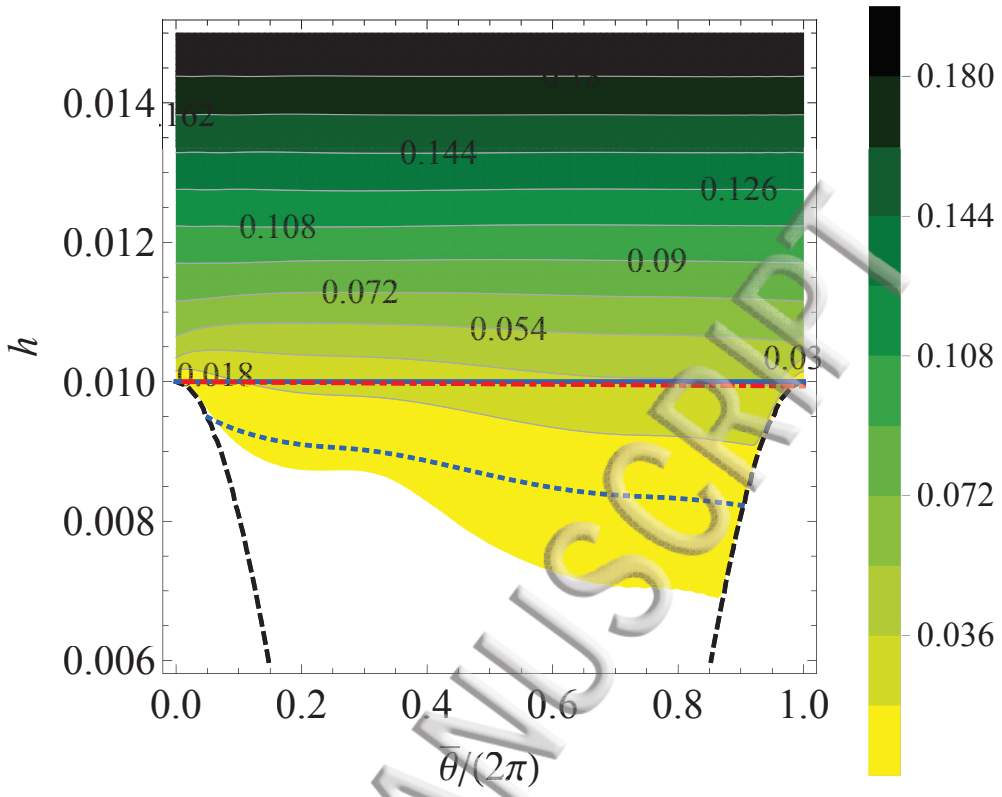

FIG. 5. Contour plot of the relative density $n(\bar{\theta}, h)/n^{(0)}(R_1)$. The black dashed line is the scrape-off layer. The solid blue line and the red dot-dashed line are the critical contours $h = h_c$ and $k = h_c$. The blue dotted line represents the diffusive broadening layer $(\Delta h)_2$.

zeroth-order equation $\partial n^{(0)}/\partial\bar{\theta} = 0$ and its simple solution $n^{(0)} = n^{(0)}(h)$.

In first order, the expansion yields the equation

$$\frac{\partial n^{(1)}}{\partial\bar{\theta}} = \frac{\partial}{\partial h}\left[\beta n^{(0)}(h) - \delta\frac{\partial h}{\partial p}\frac{\partial n^{(0)}}{\partial h}\right]. \tag{75}$$

Treating β and δ as constants and using the periodic boundary condition required for $n(\bar{\theta}, h)$ in the region $h > h_c$ yields the equation

$$0 = \int_0^{2\pi}\frac{d\bar{\theta}}{2\pi}\frac{\partial n^{(1)}}{\partial\bar{\theta}} = \frac{\partial}{\partial h}\left[\beta n^{(0)}(h) - \delta\left\langle\frac{\partial h}{\partial p}\right\rangle\frac{\partial n^{(0)}}{\partial h}\right], \tag{76}$$

where

$$\left\langle\frac{\partial h}{\partial p}\right\rangle \equiv \int_0^{2\pi}\frac{d\bar{\theta}}{2\pi}\frac{\partial h}{\partial p} = -\int_0^{2\pi}\frac{d\bar{\theta}}{2\pi}\sqrt{\cos^2\bar{\theta} + 4h}. \tag{77}$$

Here, the last expression follows from Eqs. (48) and (54).

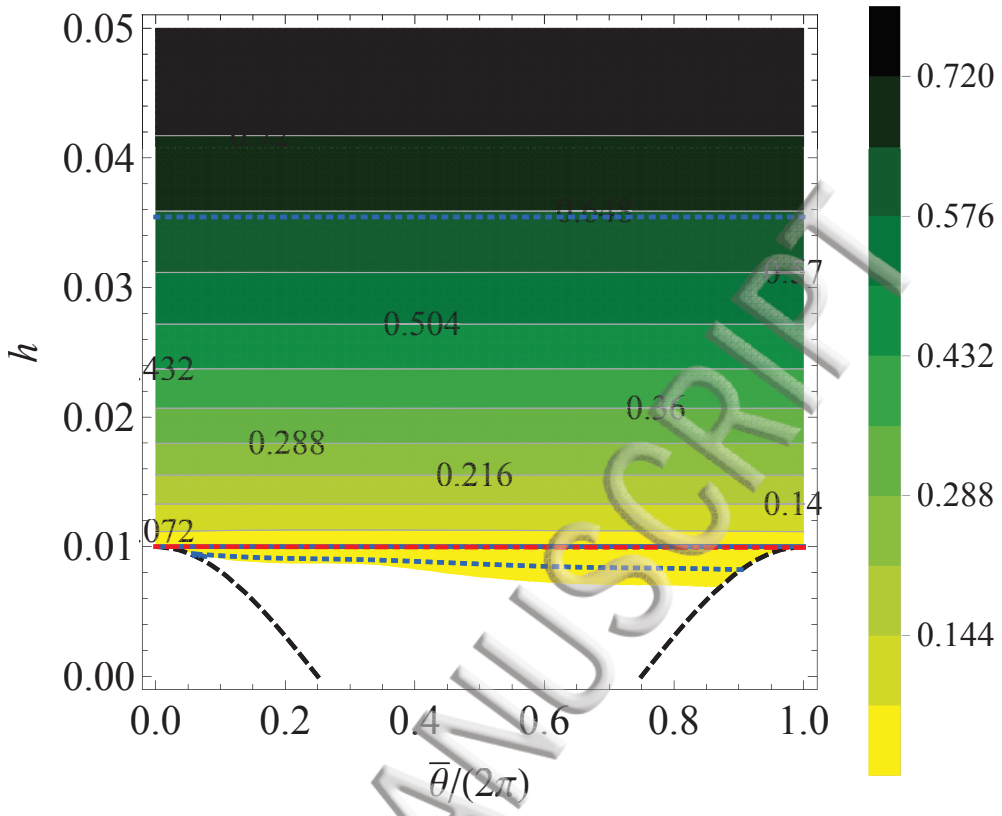

FIG. 6. Contour plot of the relative density $n(\bar{\theta}, h)/n^{(0)}(R_1)$. The black dashed line is the scrape-off layer. The solid blue line and the red dot-dashed line are the critical contours $h = h_c$ and $k = h_c$. The upper and lower blue dotted line represent the diffusive broadening layer $(\Delta h)_1$ and $(\Delta h)_2$.

Since the diffusion term will be significant only at the leading edge of the halo where $h \ll 1$, the last integral in Eq. (77) has the approximate value $\langle \partial h/\partial p \rangle \simeq -2/\pi$. Thus, Eq. (76) reduces to the simple form

$$0 = \frac{\partial}{\partial h}\left[n^{(0)}(h) + (\Delta h)_1 \frac{\partial n^{(0)}}{\partial h} \right], \tag{78}$$

where $(\Delta h)_1 = 2\delta/\pi\beta$. The solution is given by the expression

$$n^{(0)}(h) = C_1 + (C_2 - C_1) \exp\left[-\frac{h - h_c}{(\Delta h)_1} \right], \tag{79}$$

where C_1 and C_2 are constants. For $h - h_c \gg (\Delta h)_1$, the density $n^{(0)}(h)$ has the constant value C_1, which we identify as the constant $n^{(0)}(R_1)$. The constant C_2 is the value of the

$\bar{\theta}$-averaged density at $h = h_c$, $n^{(0)}(h_c)$. This latter constant must be determined by matching onto the solution for $h < h_c$.

One can continue with the perturbation analysis to determine the $\bar{\theta}$-dependent part of the density, but the conclusion is that $(\Delta h)_1$ sets the diffusive broadening scale. The upper blue dotted curve in Fig. (6) is the line $h = (\Delta h)_1 = 2\delta/\pi\beta$. Physically, this broadening scale is determined by a competition between diffusion and mobility.

In the region $0 < h < h_c$, a given particle makes a single pass through the $(\bar{\theta}, h)$ space and then is lost to the scrape-off layer, so the diffusive broadening in this region is determined by a competition between diffusion and $\mathbf{E}\times\mathbf{B}$ drift streaming. Neglecting the mobility term in Eq. (51) and using the small-h expansion $\partial h/\partial p \simeq -|\cos\bar{\theta}|$ in the diffusion term yields the diffusive broadening scale

$$(\Delta h)_2(\bar{\theta}) = [2\delta \int_0^{\bar{\theta}} d\bar{\theta}' |\cos\bar{\theta}'|]^{1/2}. \tag{80}$$

The lower dotted blue curve in Figs. (5) and (6) is a plot of $(\Delta h)_2(\bar{\theta})$. For the conditions of the experiment, $(\Delta h)_1$ is substantially larger than $(\Delta h)_2(\bar{\theta})$.

If the diffusive broadening scales $(\Delta h)_1$ and $(\Delta h)_2$ satisfy appropriate constraints, the details of the density distribution are not needed to calculate the damping rate and frequency shift. First, we require that there exists a contour $h = h_b$, where $h_b - h_c$ is a few times larger than $(\Delta h)_1$ and yet $h_b \ll 1$. This is possible if $(\Delta h)_1 \ll 1$. Recall that $h_c \simeq \Delta p \ll 1$. The density then has the constant value $n^{(0)}(R_1)$ for $h \geq h_b$.

Second, we require that $(\Delta h)_2(\bar{\theta} = 3\pi/2)$ be small compared to $h_c \simeq \Delta p$, so that particles can't reach the contour $h = 0$. Note here that the scrape-off layer on the Right Hand Side of Fig. (5) intersects the contour $h = 0$ at $\bar{\theta} = 3\pi/2$. Physically, the particles must be swept to the scrape-off layer by the $\mathbf{E}\times\mathbf{B}$ drift flow before the diffusive broadening can move the particles to $h = 0$.

In summary, the required inequalities are the following

$$(\Delta h)_1 = \frac{2\delta}{\pi\beta} = \frac{2}{\pi}\frac{T}{Ne^2}\frac{R_w}{4D} \ll 1 \tag{81}$$

$$1 \gg (\Delta p)^2 \simeq h_c^2 \gg [(\Delta h)_2(3\pi/2)]^2 = 6\delta = \frac{3}{2}\frac{T\beta}{Ne^2}\frac{R_w}{D}, \tag{82}$$

which are consistent with the experimental conditions except for the smallest values of D.

By using the constancy of $n(\bar{\theta}, h)$ for $h > h_b$, Eqs. (59) and (60) can be re-written in the

form

$$\frac{\partial D}{\partial t} = \frac{ecR_w}{B}\left(\frac{4D}{R_w}\right)^2 \int_0^{2\pi} d\bar{\theta}\sin\bar{\theta}\left\{\frac{n^{(0)}(R_1)}{2}[p_-^2(\bar{\theta},h_b) - p^2(R_1)] + \int_{h_b}^0 dh p_-(\bar{\theta},h)\frac{\partial p_-(\bar{\theta},h)}{\partial h} n(\bar{\theta},h)\right\}, \tag{83}$$

$$D\Delta\omega = -\frac{ecR_w}{B}\left(\frac{4D}{R_w}\right)^2 \int_0^{2\pi} d\bar{\theta}\cos\bar{\theta}\left\{\frac{n^{(0)}(R_1)}{2}[p_-^2(\bar{\theta},h_b) - p^2(R_1)] + \int_{h_b}^0 dh p_-(\bar{\theta},h)\frac{\partial p_-(\bar{\theta},h)}{\partial h} n(\bar{\theta},h)\right\}, \tag{84}$$

where the differential relation $dp = dh(\partial p/\partial h)_{\bar{\theta}}$ has been used in the integrals.

In both square brackets, the constant term $p_-^2(R_1)$ integrates to zero. By even-odd arguments, the term $p_-^2(\bar{\theta},h_b)$ integrates to zero in Eq. (83), but not in Eq. (84). The integral over h makes the only contribution in Eq. (83) and may be neglected in Eq. (84). The integral is negligible there because $h_b \ll 1$. Thus, the equations reduces to the form

$$\frac{\partial D}{\partial t} = \frac{ecR_w}{B}\left(\frac{4D}{R_w}\right)^2 \int_0^{2\pi} d\bar{\theta}\sin\bar{\theta}\int_{h_b}^0 dh p_-(\bar{\theta},h)\frac{\partial p_-(\bar{\theta},h)}{\partial h} n(\bar{\theta},h), \tag{85}$$

$$D\Delta\omega = -\frac{ecR_w}{B}\left(\frac{4D}{R_w}\right)^2 \frac{n^{(0)}(R_1)}{2}\int_0^{2\pi} d\bar{\theta}\cos\bar{\theta}p_-^2(\bar{\theta},h_b). \tag{86}$$

The reason that the diffusive broadening makes only a negligible change in the frequency shift is easy to understand. The leading edge of the halo has the approximate $\bar{\theta}$-dependence $p_-(\bar{\theta},0)$, which varies by order unity as $\bar{\theta}$ varies over the interval $(0,2\pi)$. On the other hand the diffusive broadening is small compared to unity, $(\Delta p_-)_{\rm broad} \simeq (\partial p_-/\partial h)(\Delta h)_1 \sim 2\delta/\pi\beta \ll 1$, so the change produced by the broadening is negligible.

To evaluate the damping rate in Eq. (85) first recognize that $p_-\sin\bar{\theta} = \partial h/\partial\bar{\theta}$, based on the form of h in Eq. (48). Such recognition, together with the chain rule $(\partial h/\partial\bar{\theta}|_{p_-})(\partial p_-/\partial h|_{\bar{\theta}}) = -\partial p_-/\partial\bar{\theta}|_h$, and an integration by parts over $\bar{\theta}$ since $p_-(\bar{\theta},h)$ and $n(\bar{\theta},h)$ are periodic in $\bar{\theta}$, allows us to rewrite Eq. (85) as

$$\frac{\partial D}{\partial t} = \frac{ecR_w}{B}\left(\frac{4D}{R_w}\right)^2 \int_0^{2\pi} d\bar{\theta}\int_{h_b}^0 dh p_-(\bar{\theta},h)\left.\frac{\partial n}{\partial\bar{\theta}}\right|_h. \tag{87}$$

Since $h_b \ll 1$, $p_-(\bar{\theta},h)$ can be approximated by $p_-(\bar{\theta},0)$, which is given by $p_-(\bar{\theta},0) = \cos\bar{\theta}$ from Eq. (54) for $\pi/2 < \bar{\theta} < 3\pi/2$ and is zero elsewhere. Thus, Eq. (87) reduces to the form

$$\frac{\partial D}{\partial t} = \frac{ecR_w}{B}\left(\frac{4D}{R_w}\right)^2 \int_{\pi/2}^{3\pi/2} d\bar{\theta}\cos\bar{\theta}\int_{h_b}^0 dh\left.\frac{\partial n}{\partial\bar{\theta}}\right|_h. \tag{88}$$

Substituting for $\partial n/\partial\bar{\theta}|_h$ from transport equation (51), carrying out the h-integral and using the relations $n(\bar{\theta}, h_b) = n^{(0)}(R_1)$ and $\partial n/\partial h(\bar{\theta}, 0) = 0$ yields the expression

$$\frac{\partial D}{\partial t} = -\frac{ecR_w}{B}\left(\frac{4D}{R_w}\right)^2 \int_{\pi/2}^{3\pi/2} d\bar{\theta}\cos\bar{\theta}\cdot\beta n^{(0)}(R_1), \tag{89}$$

which reduces to the result

$$\frac{dD}{dt} = \frac{ecR_w}{B}\left(\frac{4D}{R_w}\right)^2 n^{(0)}(R_1)\cdot 2\beta = -\frac{2}{\pi}\frac{|dN/dt|}{N}R_w, \tag{90}$$

This result is the same as the damping rate for zero-diffusion given in Eqs. (71) and (2).

This analytic solution for the damping rate approximates the $d\bar{\theta}dh$ integrals in Eq. (85), denoted as

$$J \equiv \int_0^{2\pi} d\bar{\theta}\sin\bar{\theta}\int_{h_b}^{0} dh p_- \frac{\partial p_-}{\partial h}\frac{n(\bar{\theta}, h)}{n^{(0)}(R_1)}, \tag{91}$$

by the value 2β, which significantly is independent of δ, provided δ is not too large. Fig. (7) shows a comparison of this analytical approximation for the integral J to a direct numerical evaluation using the numerical solutions for the diffusively broadened density found in Appendix A.

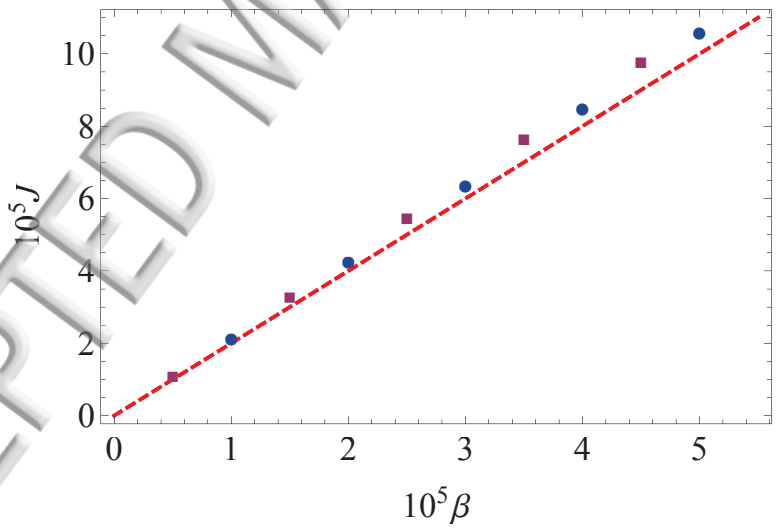

FIG. 7. Values of damping integral J. Numerical results are in squares for $T = 4\times10^{-2}Ne^2$ and in circles for $T = 1.6\times10^{-2}Ne^2$, with $D = 0.1R_w$. Red dashed line shows the approximate analytical result $J \simeq 2\beta$.

The numerical evaluations are obtained for many values of β, shown in the figure, and for $D = 0.1R_w$ and two distinct values of T, $T = 1.6\times10^{-2}Ne^2$ and $T = 4\times10^{-2}Ne^2$. These

values are characteristic of the experiment. The value of h_b is taken to be large enough that $n(\bar{\theta}, h)/n^{(0)}(R_1)$ is close to 1 and the integral J is independent of h_b.

Results for $T = 1.6 \times 10^{-2} Ne^2$ are shown as circles and for $T = 4 \times 10^{-2} Ne^2$ as squares. The red dashed line is the analytic result 2β. Significantly, the circles and squares lie close to the red line, with slightly larger values. The origin of the difference lies in the approximation made in Eq. (88) in the analytic evaluation. We neglected the small finite h in $p_-(\bar{\theta}, h)$. However, when the finite value of $0 < h < h_b$ is retained in the numerical evaluation, values slightly larger than the analytic approximation is obtained.

That diffusive broadening does not change the damping rate significantly, even when the broadening is much wider than the thin region responsible for damping in the zero-diffusive model [i.e. $(\Delta h)_1 \gg 2\pi\beta$] may be surprising. All that is needed is that $(\Delta h)_1$ and $(\Delta h)_2$ satisfy inequalities (81) and (82).

To understand the near equality of the two damping rates, first note that the scaled flow of particles through contour h_b is simply $2\pi\beta n^{(0)}(R_1)$, which is the same as the flow through contour h_c in the zero diffusion model. Provided that $(\Delta h)_2 \ll \Delta p$, all of the particles that pass through contour $h = h_b$ ultimately enter the scrape-off layer. To calculate the average change in angular momentum of the particles as they move from $h = h_b$ to the scrape-off layer, one need only replace h_c by h_b in Eq. (73). By inequality (82), h_b is small compared to unity and the modified version of Eq. (73) still reduces to the result in Eq. (74). Thus, the average rate of change of angular momentum for the particles is the same in the two cases.

The question remains as to whether or not the average rate of change of angular momentum is a good approximation to the torque exerted by the wave on the particles. In the zero diffusion model, particles cross the contour $h = h_c$ and then enter the scrape-off layer in a single pass through the $(\bar{\theta}, h)$ space. In scaled variables, the change in angular momentum of a particle caused by the transport during this period is of order $\delta p \sim \beta$, which is much smaller than the average change $\delta p \sim 1$.

In the finite diffusion case, particles cross the contour $h = h_b$ and then make many passes through the $(\bar{\theta}, h)$ space before reaching the scrape-off layer, so torque due to transport has more time to act on the particle. The change in angular momentum due to the transport is of order $\delta p \sim h_b$, which is much larger than β, but according to inequality (82) is still small compared to the average change in angular momentum $\delta p \sim 1$. Thus, the rate of change

This manuscript was accepted by Phys. Plasmas. Click here to see the version of record.

of angular momentum of the particles still provides a good approximation to the torque exerted by the wave. Therefore, the damping rates for the two cases are nearly the same.

VI. CORRECTION FOR TIME DEPENDENCE IN $D(t)$

Here, we obtain a perturbative correction to the damping rate due to the explicit time dependence in the Hamiltonian, that is, due to the time dependence in $D(t)$. Unscaled equations must be used to obtain this correction since $D(t)$ enters the scaling. The first two terms on the Left Hand Side of Eq. (41) give rise to the correction.

To estimate the relative size of these two terms, we substitute the approximate zero-diffusion solution $n(\bar{\theta}, \bar{H}, t) = n^{(0)}(R_1)\mathcal{U}[\bar{H} - \bar{H}_c(t)]$, obtaining the relation $\partial n/\partial t|_{\bar{\theta},\bar{H}} = (-\partial \bar{H}_c/\partial t)(\partial n/\partial \bar{H})_{\bar{\theta},t}$. One can show that $|\partial \bar{H}_c/\partial t|$ is small compared to $|\partial \bar{H}/\partial t|$ for $\Delta p \ll 1$, so the first term may be neglected in comparison to the second. The equation then takes the form

$$\left.\frac{\partial n}{\partial \bar{\theta}}\right|_{\bar{H},t} = \frac{\partial}{\partial \bar{H}}\left[-\dot{P}_\theta|_T\, n + \left.\frac{\partial \bar{H}}{\partial P_\theta}\right|_{\bar{\theta},t} \tilde{\mathcal{D}} \left.\frac{\partial n}{\partial \bar{H}}\right|_{\bar{\theta}}\right] + \left.\frac{\partial P_\theta}{\partial t}\right|_{\bar{H},t} \left.\frac{\partial n}{\partial \bar{H}}\right|_{\bar{\theta},t}, \tag{92}$$

where

$$\left.\frac{\partial P_\theta}{\partial t}\right|_{\bar{\theta},\bar{H}} = -\frac{\partial \bar{H}/\partial t|_{\bar{\theta},P_\theta}}{\partial \bar{H}/\partial P_\theta|_{\bar{\theta},t}} \tag{93}$$

is the rate at which a contour $\bar{H}(\bar{\theta}, P_\theta, t) =$ constant moves upward in the $(\bar{\theta}, P_\theta)$ phase space.

Anticipating that we will need Eq. (92) only for $\bar{\theta}$ in the range $\pi/2 < \bar{\theta} < 3\pi/2$ and only for small values of h, Eq. (54) implies that

$$\frac{P_\theta - P_w}{P_w} \simeq \frac{4D(t)}{R_w}\cos\bar{\theta}, \tag{94}$$

which in turn implies the relation

$$\left.\frac{\partial P_\theta}{\partial t}\right|_{\bar{\theta},\bar{H}} \simeq \frac{4\dot{D}(t)}{R_w} P_w \cos\bar{\theta}. \tag{95}$$

Changing to scaled variables, choosing an angle in the range $\pi/2 < \bar{\theta} < 3\pi/2$ and integrating with respect to h from $h = h_b$ to $h = 0$ yields the result

$$\int_{h_b}^{0} dh \left.\frac{\partial n}{\partial \bar{\theta}}\right|_{h,t} = -\beta n^{(0)}(R_1)[1 - \frac{4\dot{D}P_w}{R_w \dot{P}_\theta|_T}\cos\bar{\theta}]. \tag{96}$$

Comparing this result to Eqs. (88) and (89) shows that the square bracket is a correction to the flux through the contour $h = h_b$ to account for the the fact that the contour moves in time.

Substituting this result into Eq. (88) and carrying out the $\bar{\theta}$-integration yields the damping rate

$$\frac{dD}{dt} = -\frac{\gamma}{1 + 2N_h/N} \simeq -\gamma(1 - 2N_h/N), \tag{97}$$

where γ is the zero-diffusion damping rate in Eq. (71) and $N_h/N \simeq 0.1$.

VII. DISCUSSION

How general is the flux-driven damping mechanism discussed here? First note that the mechanism is not limited to the case of an $m = 1$ mode. Subsequent to the experimental discovery of the damping for an m=1 diocotron mode, similar damping was observed for an $m = 2$ mode[14]. Again, algebraic damping began when the halo particles reached the resonant layer, which for the $m = 2$ mode is well separated from the wall.

Because the resonant layer for the $m = 2$ mode is well separated from the wall, one may ask what plays the role of the wall in truncating particle orbits? Put another way, what prevents the resonant particles from giving back angular momentum that they have received from the mode? We believe that the answer is simply passage of the particles through the "cat's-eye" orbits in the resonant layer. Because of transport, the particles cannot come back through these structures, and in the one-way passage, the particles pick up significant angular momentum from the mode, causing the damping. In principle, this mechanism also would apply for $m = 3$ and higher, but the resonant layer is closer to and even inside the core for higher m modes, and such modes typically suffer large ordinary Landau damping.

In this paper we do not treat the damping of the $m = 2$ mode in parallel with the damping of the m=1 mode, because there are technical differences between $m = 1$ and $m = 2$ cases. The $m = 1$ mode admits an analytic solution for a general monotonically decreasing density profile, while the $m = 2$ mode does not. The structure of the "cat's-eye" orbits differ, since the potential goes to zero at the resonant radius for an $m = 1$ mode (i.e. at the wall), but not for the $m = 2$ mode. Also, the truncation of the orbits by the wall is different than simply passing through the "cats eye orbits. The theory for the higher order modes must wait for a later paper.

Broader than the flux-driven damping mechanism itself is the idea that all Landau-type damping (or growth), that is, damping (or growth) due to interaction with resonant particles, can be thought of as resulting from the action of the bare electric field from the resonant particles back on the mode. The resonant particles travel at the mode phase velocity so the electric field from the resonant particles drives the mode resonantly. The idea is not limited to the case where the azimuthal mode number is unity and the field from the resonant particles is uniform, but applies for arbitrary mode number. This general idea was elaborated in a recent paper[25].

ACKNOWLEDGMENTS

The authors gratefully acknowledge useful discussion with Dr. C. F. Driscoll, Dr. D. H. Dubin and Dr. A. A. Kabantsev.

This work was supported by National Science Foundation Grant No. PHY-1414570 and U.S. Department of Energy Grant No. DE-SC0002451.

Appendix A: Numerical solution for diffusive broadening

This appendix describes a numerical solution of the transport equation (51) using an eigenfunction expansion. This solution follows a similar approach in the work of Dubin and Tsidulko[26].

Fig. (8) illustrates the region of the solution of Eq. (51). In this figure, we set $p = \Delta p = 10^{-2}$ to be the scrape-off layer. The scrape-off layer is the black solid contour $h = \Delta p \cos\bar{\theta}$, with smaller term $(\Delta p)^2$ dropped. The critical contour, which is the blue dot-dashed curve, is $h = h_c = \Delta p$. The orange dotted curve is the contour $h = 0$.

The region for which $n(\bar{\theta}, h)$ is solved is bounded in the figure by the scrape-off layer and the straight lines $\bar{\theta} = 0$ and $\bar{\theta} = 2\pi$. It can be divided into three region of interests, which are $h > h_c$, $0 < h < h_c$ and $h < 0$. The three regions are to be explained in the paragraphs that follow. Meanwhile three boundary conditions of Eq. (51) will be introduced in the explanation.

The first region, $h > h_c$, is taken to extend to infinite h, since we are interested in the regime $h < h_b \ll 1$ and the non-resonant region is far from the wall. At large h, the density

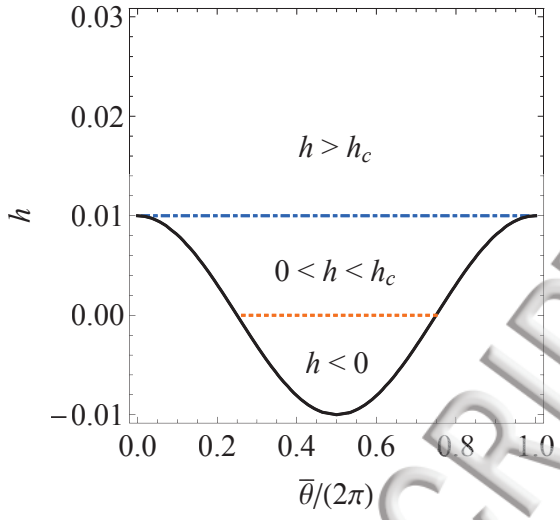

FIG. 8. Illustration of the region for which Eq. (51) is solved. The black solid curve is the scrape-off layer. The blue dot-dashed curve is the critical contour $h = h_c$. The orange dotted curve is the contour $h = 0$.

is equal to that at the edge of the non-resonant region. Therefore

$$\lim_{h\to\infty} n(\bar{\theta}, h) = n^{(0)}(R_1), \tag{A1}$$

which is our first boundary condition.

Our second boundary condition is the periodic boundary condition $f(\bar{\theta} = 0, h) = f(\bar{\theta} = 2\pi, h)$, as $\bar{\theta} = 0$ and $\bar{\theta} = 2\pi$ refers to the same physical point. It only applies in the region $h > h_c$, which is the only region that can access $\bar{\theta} = 0$ and $\bar{\theta} = 2\pi$.

The second region, $0 < h < h_c$, is the region of open orbits in contact with the scrape-off layer, where the density must be zero, i.e.

$$n(\bar{\theta}, h = \Delta p \cos\bar{\theta}) = 0. \tag{A2}$$

In this region, the range of $\bar{\theta}$ that a particle can access is bounded by the scrape-off layer.

The third region, $h < 0$, differs from the first and second region in that the contours are closed in this region. We continue to apply Eq. (51) in this region, and use the same zero-density boundary $h = \Delta p \cos\bar{\theta}$ as in the second region. However in Eq. (51), the factor $\partial h/\partial p$ takes $p = p_-(\bar{\theta}, h)$ from Eq. (54) when $p(\bar{\theta}, h)$ is expressed, and misses the $p = p_+(\bar{\theta})$ part of the closed contour for $h < 0$. Fortunately, the error is negligible because this region is dynamically inaccessible to the particles, as discussed in the small-diffusion condition (82)

in section V. There are literally no particles for $h < 0$, and thus n is vanishingly small in this region.

Since Eq. (51) is linear and the boundary conditions are homogeneous, the density may be normalized as $f \equiv n/n^{(0)}(R_1)$ and the equation rewritten as

$$\left.\frac{\partial f}{\partial \bar{\theta}}\right|_h = \frac{\partial}{\partial h}[\beta f - \delta \left.\frac{\partial h}{\partial p}\right|_{\bar{\theta}} \left.\frac{\partial f}{\partial h}\right|_{\bar{\theta}}]. \tag{A3}$$

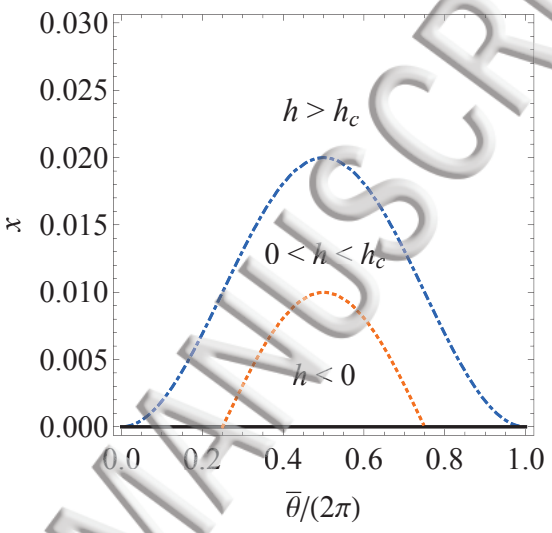

FIG. 9. Illustration of the region of solution in $(\bar{\theta}, x)$-space. The black solid line is the scrape-off layer. The blue dot-dashed curve is the critical contour $h = h_c$. The orange dotted curve is the contour $h = 0$.

In order to fit the boundary condition more easily, we change variables from $(\bar{\theta}, h)$ to $(\bar{\theta}, x)$, where $x \equiv h - \Delta p \cos\bar{\theta}$. Fig. (9) shows the region of solution in the $(\bar{\theta}, x)$ space. The black solid line is the scrape-off layer. The blue dot-dashed curve is the critical contour $h = h_c$ and the orange dotted curve is the contour $h = 0$. As we see from the figure, the region of solution in Fig. (8) is reshaped to the semi-infinite rectangular region in Fig. (9). The boundaries of the region of solution are lines $x = 0$, $\bar{\theta} = 0$, and $\bar{\theta} = 2\pi$, and the region extends to infinite x. As discussed when the region was described in $(\bar{\theta}, h)$-space, the solution is solved considering the three subregions $h > h_c$, $0 < h < h_c$ and $h < 0$ as a whole, although we expect the value of f in the dynamically inaccessible region $h < 0$ to be vanishingly small.

In this new set of variables and the normalized density, the first boundary condition,

which is the large-h limit (A1), is expressed as

$$\lim_{x\to\infty} f = 1. \tag{A4}$$

The second boundary condition, which is the periodic boundary condition, is rephrased as $f(\bar{\theta}=0,x) = f(\bar{\theta}=2\pi,x)$. It applies only to the region $h > h_c$, the same as when the region was described in terms of $(\bar{\theta}, h)$. Since the region $h > h_c$ reaches all values of $x > 0$, the periodic boundary condition applies for all $x > 0$.

More importantly, at the scrape-off layer, the third boundary condition (A2) is now expressed as

$$f(\bar{\theta}, x=0) = 0, \tag{A5}$$

which is much easier to work with as the scrape-off layer is straightened to be the horizontal line $x = 0$, and $\bar{\theta}$-dependence is avoided.

By using the relations $\partial_h|_{\bar{\theta}} = (\partial x/\partial h)\partial_x|_{\bar{\theta}}$ and $\partial_{\bar{\theta}}|_h = (\partial x/\partial\bar{\theta})\partial_x|_{\bar{\theta}} + \partial_{\bar{\theta}}|_x$ Eq. (A3) is rewritten in the form

$$\left.\frac{\partial f}{\partial\bar{\theta}}\right|_x + \Delta p \sin\bar{\theta}\left.\frac{\partial f}{\partial x}\right|_{\bar{\theta}} = \frac{\partial}{\partial x}[\beta f - \delta\cdot\eta(x,\bar{\theta})\left.\frac{\partial f}{\partial x}\right|_{\bar{\theta}}]. \tag{A6}$$

Here $\eta(\bar{\theta}, x) \equiv \partial h/\partial p$ is explicitly expressed as

$$\eta(\bar{\theta}, x) = -\sqrt{\cos^2\bar{\theta} + 4h(\bar{\theta}, x)} \tag{A7}$$

using the relations (48) and (54). The fact that we are interested in the region $0 < h < h_b \ll 1$ permits us to remove the x-dependence in η by neglecting h and thus approximating

$$\eta(\bar{\theta}, x) \simeq \eta(\bar{\theta}) \equiv -|\cos\bar{\theta}|. \tag{A8}$$

Since $f(\bar{\theta}, x)$ and $\eta(\bar{\theta})$ are both periodic in $\bar{\theta}$ for all values of x, they may be expressed as the Fourier Series

$$f(\bar{\theta}, x) = \sum_{\mu=-\infty}^{+\infty} f_\mu(x) e^{i\mu\bar{\theta}}, \tag{A9}$$

$$\eta(\bar{\theta}) = \sum_{\nu=-\infty}^{+\infty} \eta_\nu e^{i\nu\bar{\theta}}, \tag{A10}$$

where $\eta_\nu = -\int_0^{2\pi} d\bar{\theta}|\cos(\bar{\theta})|e^{-i\nu\bar{\theta}}/(2\pi)$. Note that $f_{-\mu} = f_\mu^*$ and $\eta_{-\nu} = \eta_\nu^*$ as f and η are real functions. In practice, both series must be truncated when solving numerically for [i.e.

$f_\mu = 0$ if $|\mu| > N_f$, and $\eta_\nu = 0$ if $|\nu| > N_\eta$]. N_f and N_η are positive integers chosen to be sufficiently large to resolve $\eta(\bar{\theta})$ and to obtain a converged solution of $f(\bar{\theta}, x)$.

Substituting Fourier expansions (A9) and (A10) into Eq. (A6), using the relation $\sin\bar{\theta} = (e^{i\bar{\theta}} - e^{-i\bar{\theta}})/(2i)$ and equating coefficients of $e^{i\mu\bar{\theta}}$ on both sides yields the differential equations

$$i\mu f_\mu(x) + i\frac{\Delta p}{2}[f'_{\mu+1}(x) - f'_{\mu-1}(x)] = \beta f'_\mu(x) - \delta \sum_{\nu=-N_\eta}^{N_\eta} \eta_{-\nu} f''_{\mu+\nu}(x). \tag{A11}$$

This is a set of $2N_f+1$ linear coupled ODEs, as the subscript μ counts from $-N_f$ to N_f. Since the coefficients are constants, we seek a solution of the form $f_\mu(x) = C_\mu e^{-sx}$. Substituting this form of solution into Eq. (A11) yields a set of eigenvalue equations

$$i\mu C_\mu - is\frac{\Delta p}{2}[C_{\mu+1} - C_{\mu-1}] = -s\beta C_\mu + s^2\delta \sum_{\nu=-N_\eta}^{N_\eta} \eta_{-\nu} C_{\mu+\nu}, \tag{A12}$$

with s as the eigenvalue and C_μ as the μ-th element of the eigenvector. By inspection, there is an obvious eigenvalue $s = 0$ with the coefficient $C_\mu = \delta_{\mu 0}$ as the eigenvector. This eigenvector corresponds to the a constant eigenfunction $f_\mu(x) = \delta_{\mu 0}$, and we set C_0 to be 1 so as to satisfy Eq. (A4) for large x. Other physically admissible eigenvalues are the ones with positive real parts, denoted as $\{s_r\}$ with the eigenvector $\{C_{\mu,r}\}$, since the eigenfunctions die out in the form of $e^{-\mathrm{Re}[s_r]x} e^{-i\mathrm{Im}[s_r]x}$ when x is large. The subscript r refers to the r-th eigenvalue and eigenvector.

Both the eigenvalues and the eigenvectors are obtained numerically. It is noteworthy that in the numerical solutions, the eigenvalue with the smallest positive real part is equal to $\pi\beta/(2\delta)$, which is the reciprocal of the diffusive broadening scale $(\Delta h)_1$ in Eq. (81). Its eigenfunction, which then has the form $e^{-x/(\Delta h)_1}$, is responsible for the change of density over that broadening region. Other eigenvalues are not as recognizable though, and the respective eigenfunctions superpose, together with that for the scale $(\Delta h)_1$, to produce the delicate density structure around $h = h_c$ in Fig. (6).

The total solution is a superposition of all the eigenfunctions

$$f(\bar{\theta}, x) = 1 + \sum_r \sum_{\mu=-N_f}^{N_f} A_r C_{\mu,r} e^{-s_r x} e^{i\mu\bar{\theta}}, \tag{A13}$$

where A_r is the coefficient of the r-th eigenfunction.

We have to satisfy the boundary condition at the scrape-off layer, therefore by following Eq. (A5), we obtain the condition

$$0 = f(\bar{\theta}, x = 0) = 1 + \sum_r \sum_{\mu=-N_f}^{N_f} A_r C_{\mu,r} e^{i\mu\bar{\theta}}. \tag{A14}$$

Collecting coefficients for every Fourier component yields the set of coupled equations

$$0 = \delta_{\mu 0} + \sum_r A_r C_{\mu,r} \tag{A15}$$

from which $\{A_r\}$ is solved numerically.

REFERENCES

[1]R. C. Davidson, in *Physics of nonneutral plasmas* (Imperial College Press, 2001) Chap. 6, pp. 289–343.

[2]R. Levy, Phys. Fluids **8**, 1288 (1965).

[3]C. Driscoll and K. Fine, Phys. Fluids B **2**, 1359 (1990).

[4]J. Fajans, E. Gilson, and L. Friedland, Phys. Rev. Lett. **82**, 4444 (1999).

[5]R. Briggs, J. Daugherty, and R. Levy, Phys. Fluids **13**, 421 (1970).

[6]W. D. White, J. H. Malmberg, and C. F. Driscoll, Phys. Rev. Lett. **49**, 1822 (1982).

[7]R. C. Davidson and E. H. Chao, Phys. Plasmas **3**, 3279 (1996).

[8]A. Kabantsev and C. Driscoll, Fus. Sci. and Tech. **51**, 96 (2007).

[9]D. Schecter, D. Dubin, A. Cass, C. Driscoll, I. Lansky, and T. O'Neil, Phys. Fluids **12**, 2397 (2000).

[10]S. Crooks and T. ONeil, Phys. Plasmas **2**, 355 (1995).

[11]B. Cluggish and C. Driscoll, Phys. Rev. Lett. **74**, 4213 (1995).

[12]E. Sarid, E. P. Gilson, and J. Fajans, Phys. Rev. Lett. **89**, 105002 (2002).

[13]A. Kabantsev, C. Driscoll, T. Hilsabeck, T. O'Neil, and J. Yu, Phys. Rev. Lett. **87**, 225002 (2001).

[14]A. Kabantsev, C. Chim, T. O'Neil, and C. Driscoll, Phys. Rev. Lett. **112**, 115003 (2014).

[15]C. Y. Chim and T. M. O'Neil, in *NON-NEUTRAL PLASMA PHYSICS IX: 11th International Workshop on Non-Neutral Plasmas*, Vol. 1668, edited by H. Himura, A. Sanpei, and Y. Soga (AIP Publishing, 2015) p. 020004.

[16]T. M. ONeil, Phys. Fluids **23**, 2216 (1980).

[17]T. M. O'Neil and R. A. Smith, Phys. Fluids B **4**, 2720 (1992).

[18]R. Levy, Phys. Fluids **11**, 920 (1968).

[19]J. Taylor, Phys. Fluids **7**, 767 (1964).

[20]T. O'Neil and R. Smith, Phys. Plasmas **1**, 2430 (1994).

[21]H. Goldstein, C. Poole, and J. Safko, in *Classical mechanics* (Addison–Wesley, 2002) Chap. 8, pp. 334–367, 3rd ed.

[22]H. Goldstein, C. Poole, and J. Safko, in *Classical mechanics* (Addison–Wesley, 2002) Chap. 9, pp. 368–429, 3rd ed.

[23]C. Driscoll, K. Fine, and J. Malmberg, Phys. Fluids **29**, 2015 (1986).

[24]M. Balkanski and R. F. Wallis, in *Semiconductor physics and applications*, Vol. 8 (Oxford University Press, 2000) Chap. 8, pp. 159–160.

[25]C. Y. Chim and T. M. O'Neil, Phys. Plasmas **23**, 050801 (2016).

[26]D. H. Dubin and Y. A. Tsidulko, Phys. Plasmas **18**, 062114 (2011).

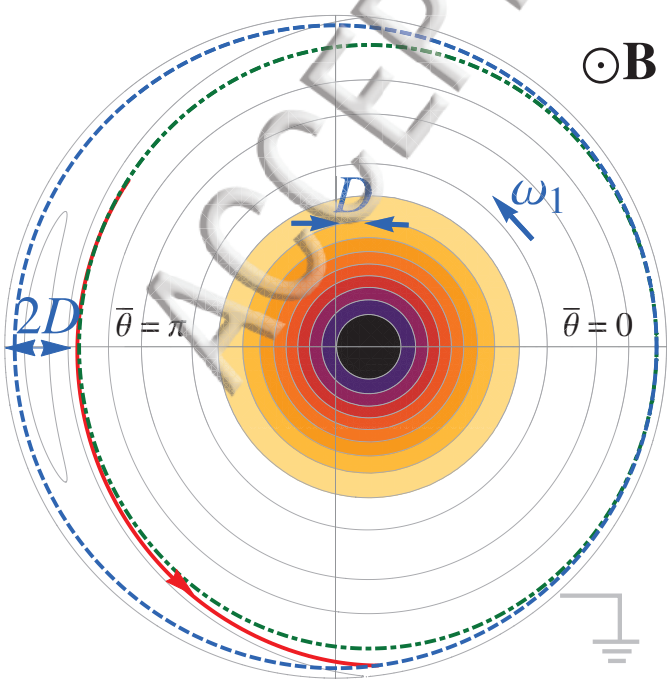
⊙B
D
ω1
2D
θ̄ = π
θ̄ = 0

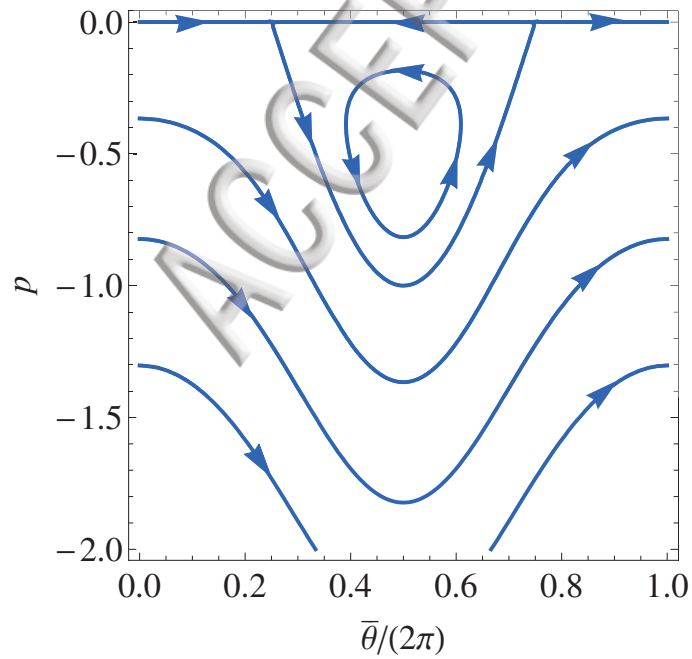
0.0
−0.5
−1.0
−1.5
−2.0
p
0.0
0.2
0.4
0.6
0.8
1.0
$\bar{\theta}/(2\pi)$

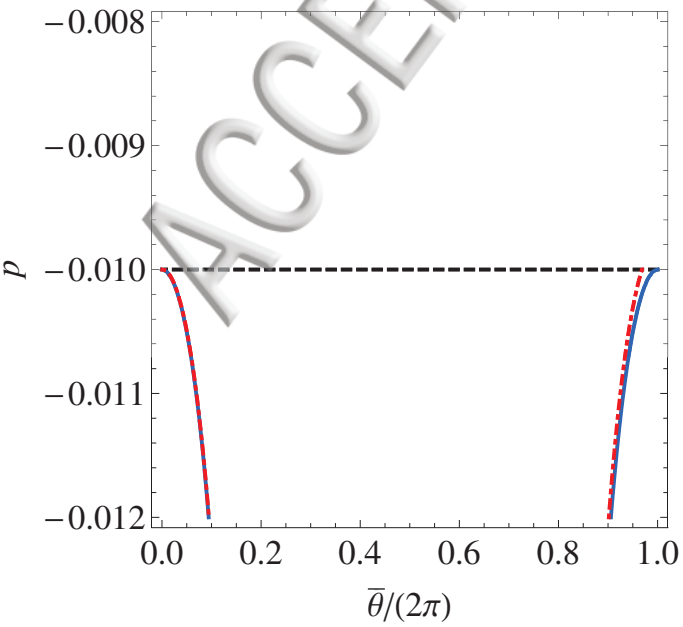
−0.008
−0.009
−0.010
−0.011
−0.012
p
0.0
0.2
0.4
0.6
0.8
1.0
θ̄/(2π)

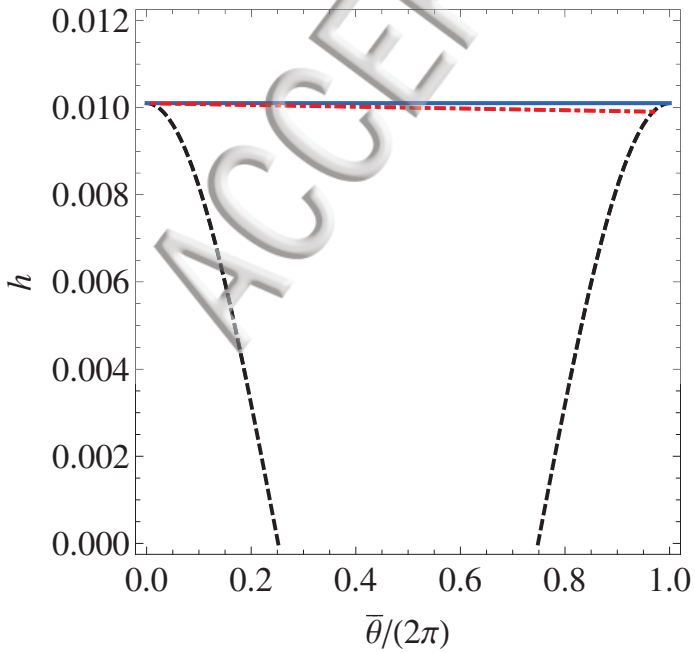
0.012
0.010
0.008
0.006
0.004
0.002
0.000
h
0.0
0.2
0.4
0.6
0.8
1.0
θ̄/(2π)

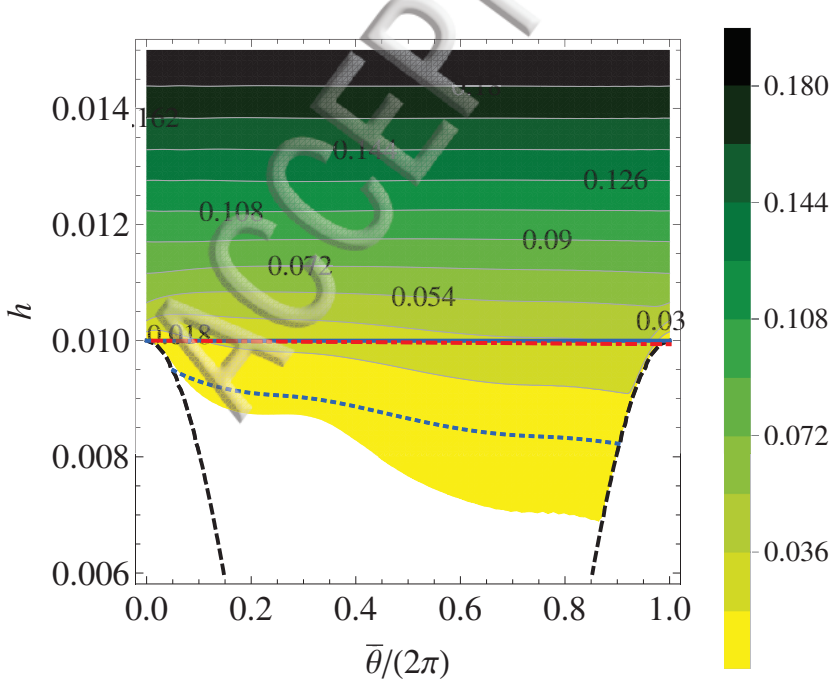
0.014
0.012
0.010
0.008
0.006
h
0.0
0.2
0.4
0.6
0.8
1.0
$\overline{\theta}/(2\pi)$
0.126
0.108
0.09
0.072
0.054
0.03
0.018
0.180
0.144
0.108
0.072
0.036

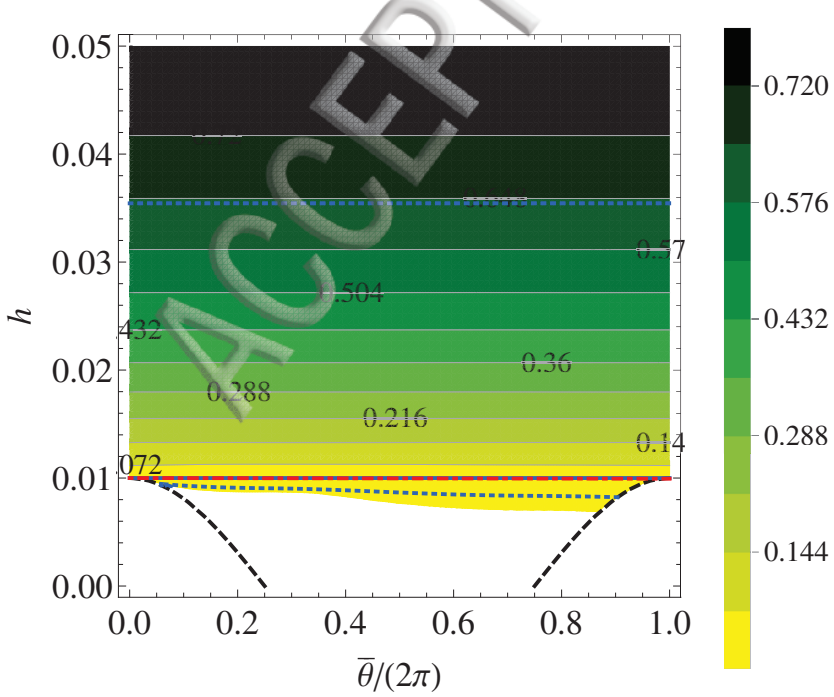
0.05
0.04
0.03
0.02
0.01
0.00
h
0.0
0.2
0.4
0.6
0.8
1.0
θ̄/(2π)
0.720
0.576
0.432
0.288
0.144
.504
0.36
0.288
0.216
0.14
072

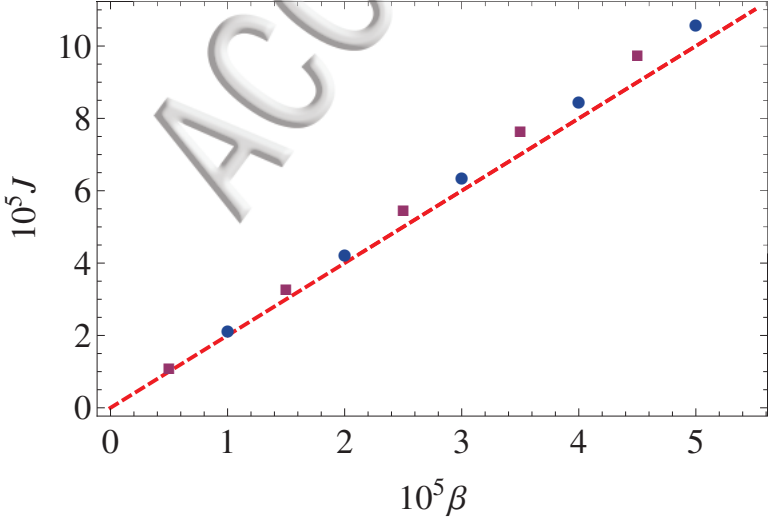
$10^5 J$
$10^5 \beta$
0
2
4
6
8
10
0
1
2
3
4
5

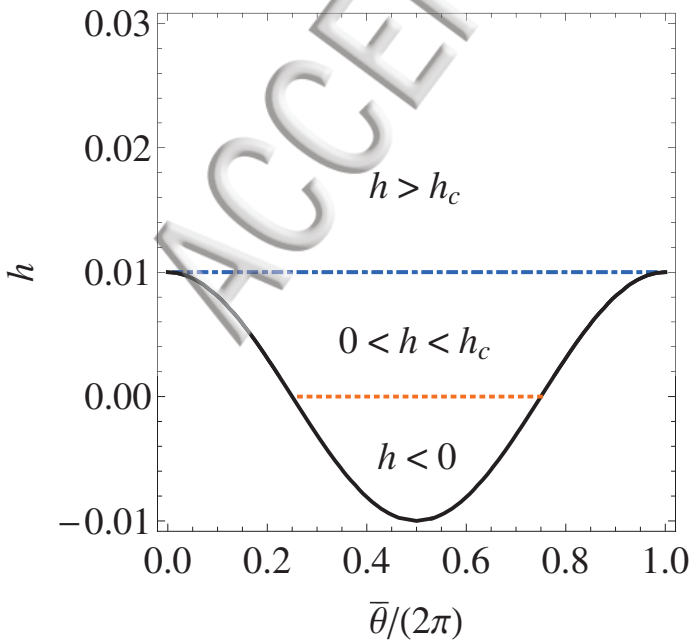
0.03
0.02
0.01
0.00
−0.01
h
0.0
0.2
0.4
0.6
0.8
1.0
$\overline{\theta}/(2\pi)$
$h > h_c$
$0 < h < h_c$
$h < 0$

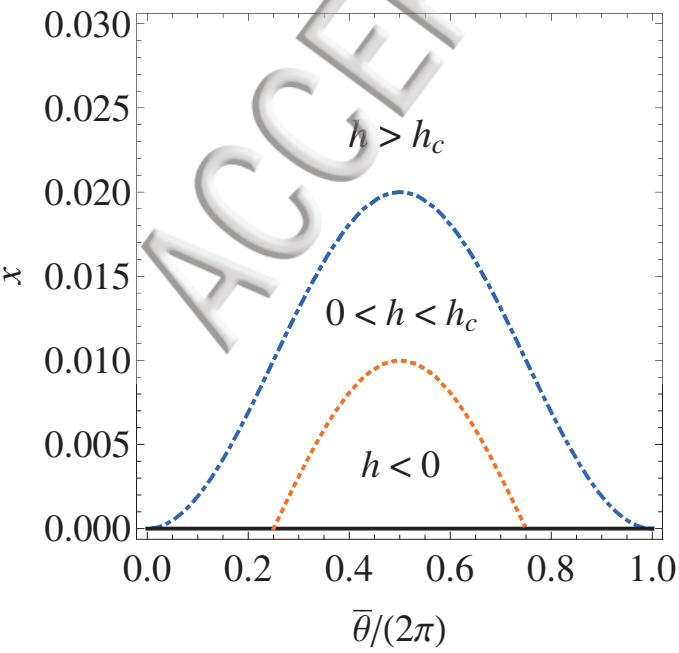
0.030
0.025
0.020
0.015
0.010
0.005
0.000
x
$h > h_c$
$0 < h < h_c$
$h < 0$
0.0
0.2
0.4
0.6
0.8
1.0
$\overline{\theta}/(2\pi)$